Analysis of Aeration Efficiency of Dissolved Oxygen through Hydraulic Jump in Rectangular Channel

A thesis submitted towards partial fulfilment of the requirements for the degree of

Master of Engineering
in
Water Resources and Hydraulic Engineering

Submitted by

INDRAJIT BERA

Exam Roll No. – M4WRE22017
Registration No. – 154657 of 2020 - 2021

Under the guidance of

Dr. SUBHASISH DAS
Associate Professor
School of Water Resources Engineering, Jadavpur University
&
Dr. RAJIB DAS
Assistant Professor
School of Water Resources Engineering, Jadavpur University

School of Water Resources Engineering
M.E. (Water Resources & Hydraulic Engineering)
*Course affiliated to **Faculty Council of Engineering & Technology***
Jadavpur University

Kolkata-700032, West Bengal, India
2022

Declaration of Originality and Compliance of Academic Ethics

I hereby declare that this thesis contains a literature survey and original research work by the undersigned candidate, as part of my **Master of Engineering** in **Water Resources and Hydraulic Engineering** in the Faculty Council of Interdisciplinary Studies, Law & Management, Jadavpur University during the academic session 2021-22.

All information in this document have been obtained and presented in accordance with academic rules and ethical conduct.
I also declare that, as required by these rules and conduct, I have fully cited and referenced all material and results that are not original to this work.

Name	**:**	**Indrajit Bera**
Exam Roll Number	**:**	**M4WRE22017**
Thesis Title	**:**	**Analysis of Aeration Efficiency of Dissolved Oxygen through Hydraulic Jump in Rectangular Channel**
Signature with Date	**:**	

M.E. (Water Resources & Hydraulic Engineering)
course affiliated to
Faculty Council of Engineering & Technology
Jadavpur University
Kolkata, India

Certificate of Recommendation

This is to certify that the thesis entitled "**Analysis of Aeration Efficiency of Dissolved Oxygen through Hydraulic Jump in Rectangular Channel**" is a Bonafide work carried out by **Mr. Indrajit Bera** under our supervision and guidance for partial fulfilment of the requirement for the Post Graduate Degree of Master of Engineering in Water Resources and Hydraulic Engineering during the academic session 2021-22.

THESIS ADVISOR

Dr. Subhasish Das

Associate Professor

School of Water Resources Engineering

Jadavpur University

THESIS ADVISOR

Dr. Rajib Das

Assistant Professor

School of Water Resources Engineering

Jadavpur University

DIRECTOR

Prof. (Dr.) Pankaj Kumar Roy

School of Water Resources Engineering

Jadavpur University

DEAN

Prof. (Dr.) Subenoy Chakraborty

Faculty Council of Interdisciplinary Studies, Law & Management
Jadavpur University

M.E. (Water Resources & Hydraulic Engineering)
course affiliated to
Faculty Council of Engineering & Technology
Jadavpur University
Kolkata, India

CERTIFICATE OF APPROVAL **

This foregoing thesis is hereby approved as a credible study of an engineering subject carried out and presented in a manner satisfactorily to warranty its acceptance as a prerequisite to the degree for which it has been submitted. It is understood that by this approval the undersigned do not endorse or approve any statement made or opinion expressed or conclusion drawn therein but approve the thesis only for the purpose for which it has been submitted.

Committee of

Final Examination

for the evaluation

of the thesis

** Only in case the thesis is approved.

ACKNOWLEDGEMENTS

I express my sincere gratitude to my supervisors, ***Dr. Subhasish Das,*** *Associate Professor, and* ***Dr. Rajib Das,*** *Assistant Professor of School of Water Resources Engineering, Jadavpur University, under whose supervision and guidance this work has been carried out. It would have been impossible to carry out this thesis work with confidence without their wholehearted involvement, advice, support and constant encouragement throughout. They have not only helped me in carrying out my thesis but also have given me valuable advice to proceed further in my life.*

I would also express my sincere gratitude to ***Prof. (Dr.) Asis Mazumdar****,* ***Prof. (Dr). Pankaj Kumar Roy*** *and* ***Dr. Gourab Banerjee****, faculty members of the School of Water Resources Engineering, Jadavpur University for their valuable suggestions.*

I also express my sincere thanks to ***Mr. Buddhadev Nandi & Mr. Saikat Mondal,*** *Research Scholars of School of Water Resources Engineering, Jadavpur University for their unconditional support and affection during my work.*

Thanks, are also due to all staff of the School of Water Resources Engineering and the Regional -cum-Facilitation Centre (RCFC), NMPB, Jadavpur University for their help and support.

Date :

Place : Jadavpur University

Mr. Indrajit Bera
(Exam Roll No: M4WRE22017)

ABSTRACT

The amount of dissolved oxygen (DO) content in a water body is one of the most important parameters to determine the water quality and hence a measure of the ability of water to sustain aquatic life. Micro-organisms such as bacteria need a high concentration of oxygen in the water to the ability to continue their lives healthfully. In this case, the concentration of the DO in the water body should be greater than 5 mg/l. A hydraulic jump is formed whenever there is a rapid or sudden change of flow from a super-critical to sub-critical flow in an open channel. Oscillating jump is detected in channels, canals below sluiceways, at the spillway bases, or during an immediate decrease in a slope like steep to flatter. In such transition, the water surface suddenly rises, surface rollers are simultaneously formed, the air is rapidly entrained, extreme mixing occurs, and energy is dissipated. The hydraulic jump is used as an effective natural mechanic mixer for the oxygen transfer and it can increase the amount of DO in the water by creating turbulent conditions. The main reason for this oxygen transfer is the air entrainment into the flow through a large number of air bubbles that helps in air-water transfer. To design and implement a hydraulic arrangement wherein a hydraulic jump is developed, it is important to identify the jump position and jump length and the quantum of energy to be disseminated.

The present study investigates the effect of hydraulic jumps on their aeration efficiency and energy dissipation. The hydraulic jump is studied as an aeration agent. Hydraulic jump, herein, is formed by adjusting a tail gate in a rectangular flume. In the study, several experiments are carried out to find out the jump characteristics and the aeration efficiency while the jump is made to occur at five different discharges ranging from 15 lps to 35 lps and three different bed slopes (horizontal, 3° and 6°). Experiments are done by varying the discharge and bed slope of water from minimum to maximum within the range of measurement and different jump characteristics are observed. The DO was measured at the water surface level throughout the jump profile. The dependence of jump parameters with varying discharge and bed slope is measured and quantified. The DO was measured using a hand-type oxygen meter. With the variation of these parameters the jump height, jump length, and DO vary. The observations and outcomes reveal a linear relationship between the aeration efficiency and energy dissipation rate. The hydraulic jump attained an aeration efficiency of 0.4175. From these results, the hydraulic jump is found to be efficient for oxygen transfer and energy dissipation. This new procedure could have practical implications for predicting hydraulic jump aeration efficiency. This study may find applications where changing stream water DO significantly affect the jump characteristics.

CONTENT

CHAPTER 1

1.1. Introduction

Hydraulic jump is one subject which has extensively been studied in the field of hydraulic engineering. It is an intriguing and interesting phenomenon that has caught the imagination of many research workers since its first description by Leonardo da Vinci. The Italian engineer Bidone (1820) conducted the first experimental investigation of this phenomenon. Since then, considerable research effort has gone into the study of this subject. The literature on this topic is vast and ever-expanding. The main reason for such continued interest in this topic is its immense practical utility in hydraulic engineering and allied fields. A hydraulic jump primarily serves as an energy dissipator to dissipate the excess energy of flowing water downstream of hydraulic structures, such as spillways and sluice gates. Some of the other uses are: (a) efficient operation of flow-measurement flumes, (b) mixing of chemicals, (c) to aid intense mixing and gas transfer in chemical processes, (d) in the desalination of seawater, and (e) in the aeration of streams which are polluted by bio-degradable wastes.

A hydraulic jump occurs when a supercritical stream meets a subcritical stream of sufficient depth. The supercritical stream jumps up to meet its alternate depth. While doing so it generates considerable disturbances in the form of large-scale eddies and a reverse flow roller with the result that the jump falls short of its alternate depth. Figure 1.1 is a schematic sketch of a typical hydraulic jump in a horizontal channel. Section 1, where the incoming supercritical stream undergoes an abrupt rise in the depth forming the commencement of the jump, is called the toe of the jump. The jump proper consists of a steep change in the water-surface elevation with a reverse flow roller on the major part. The roller entrains a considerable quantity of air and the surface has the white, frothy and choppy appearance. The jump, while essentially steady, will normally oscillate about a mean position in the longitudinal direction and the surface will be uneven. Section 2, which lies beyond the roller and with an essentially level water surface is called the end of the jump and the distance between Sections 1 and 2 is the length of the jump, Lj. The initial depth of the supercritical stream is y_1 and y_2 is the final depth, after the jump, of the subcritical stream. As indicated earlier, y_2 will be smaller than the depth alternates to y_1. The two depths y_1 and y_2 at the ends of the jump are called sequent depths. Due to the high turbulence and shear action of the roller, there is a considerable loss of energy in the jump between Sections 1 and 2. In view of the high energy loss, the nature of which is difficult to estimate, the energy equation cannot be applied to Sections 1 and 2 to relate the various flow parameters. In such situations, the use of the momentum equation with suitable assumptions is advocated. The hydraulic jump is a typical example where judicious use of the momentum equation yields meaningful results.

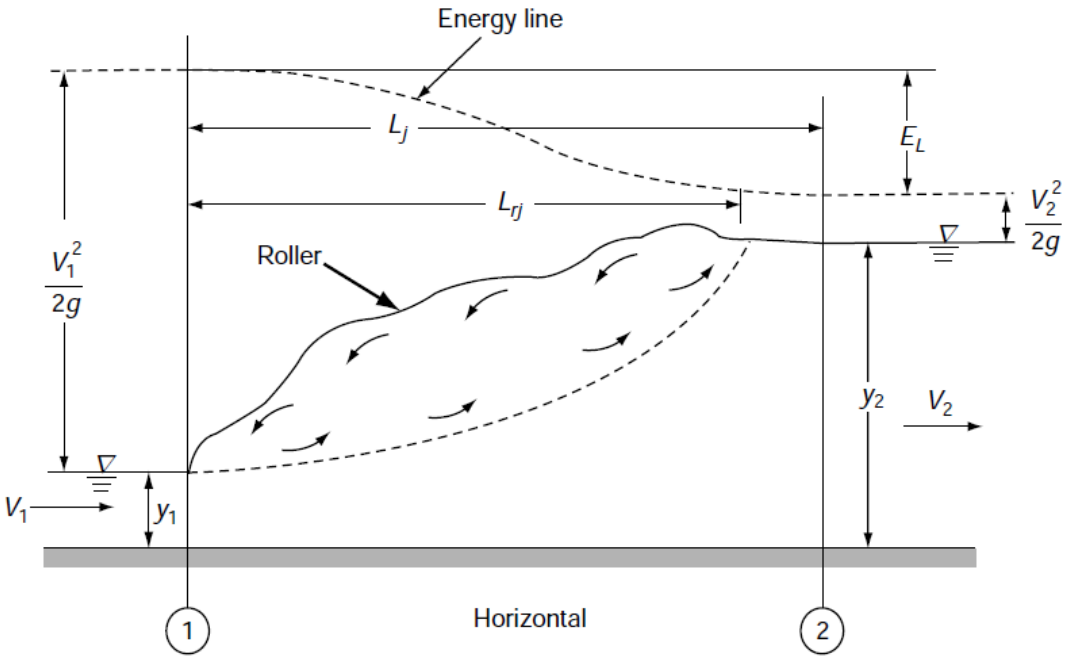

Fig. 1.1 Definition sketch of a hydraulic jump

CHAPTER 2

2.1. Literature Review

Several studies have been carried out with the purpose of predicting hydraulic jump, aeration, and flow characteristics around structures and various have been developed by various researchers. Reviews on some important experimental works were carried out by Wilhelms and Smith (1981), Wihelms *et al*. (1993), Chamson and Toombes (2002), Toombes and Chanson (2005), Kucukali and Cokgor (2009), Pagliara *et al.* (2010.), Tammela *et al.* (2010), Bostan *et al.* (2013), Raikar and Kamatagi (2015), Kim *et al.* (2016), Eltoukhy (2016), Jaiswal and Goel (2019), Hoque and Paul (2022).

Wilhelms and Smith (1981) studied the objective of this report to familiarize field reports between the oxygen transfer process and the oxygen transfer characteristics of various slow-head hydraulic structures. The physics of gas transfer is conceptually explained and the mathematical description of the gas transfer process is developed. The important physical processes and their impact on the variables in the gas transfer equation are identified. The hydraulic conditions that contribute to these physical processes are described and applied to oxygen transfer, or re-aeration.

It is hoped that field engineers, when familiar with the conceptual descriptions provided in this report, can qualitatively evaluate the oxygen transfer characteristics at a structure solely based on observed hydraulic conditions, e.g., they will be able to estimate whether the structure, upon testing, would exhibit a large or small degree of gas transfer. With the mathematical description of oxygen transfer at a "generic" type of structure and an understanding of how hydraulic conditions contribute to oxygen transfer, field engineers should be able to "bracket" or roughly estimate the transfer that is occurring at a specific structure. The hydraulic structures at most low-head projects usually consist of a gated sill, gated low-head spillway, and a fixed- or adjustable crest weir. The gas transfer analyses reported herein emphasize these "generic" types of structures.

Wihelms *et al.* (1993) investigated the gas transfer characteristics of hydraulic jumps and examined relationships which might provide a basis for quantifying the re-aeration rates or gas losses. The gas transfer occurring in several hydraulic jumps with Froude numbers ranging from 1.5 to 9.5 was measured with a gaseous tracer technique. Discharge per unit width of 0.261, 0.330, and 0.462 cubic feet per second per foot (0.0243, 0.0307, and 0.0429 $m^3/s/m$) were tested for the stated Froude number range. The relationships of gas transfer, Froude number, unit discharge, and Reynolds number were examined. A table of factors for converting U.S. customary units of measurement to metric (SI) units was presented.

Chamson and Toombes (2002) investigated that the interactions between turbulent water and the atmosphere may lead to strong air-water mixing. This experimental study is focused on the flow down a staircase channel characterised by very strong flow aeration and turbulence. Interfacial aeration is characterised by strong air-water mixing extending down to the invert. The size of entrained bubbles and droplets extends over several orders of magnitude, and a significant number of bubble/droplet clusters was observed. Velocity and turbulence intensity measurements suggest high levels of turbulence across the entire air-water flow. The increase in turbulence levels, compared to single-phase flow situations, is proportional to the number of entrained particles.

Toombes and Chanson (2005) investigated the stepped waterways which are commonly used for river training, debris dam structures, stormwater systems, and aeration cascades.

They focused on the analysis of basic air-water flow properties on a low gradient stepped chute, combined with dissolved oxygen measurements. The oxygen aeration efficiency was found to be about 30% for 12 steps with a total drop in invert elevation of 1.4 m, nearly independently of the inflow conditions. Detailed air-water flow measurements, including void fraction, velocity, bubble count rate, and interface area, were used to integrate the mass transfer equation and to estimate the aeration potential of the waterway. Direct comparisons with dissolved oxygen measurements showed good agreement between the two methods.

Kucukali and Cokgor (2009) investigated experimentally that hydraulic jumps, plunging jets and stepped channels are generally used as energy dissipators and self-aerators. Accordingly, it is expected to find a positive correlation between aeration efficiency and energy dissipation. For this purpose, hydraulic jump self-aeration efficiency was investigated with the function of energy dissipation rate per unit width. The hydraulic jump data revealed a positive linear relationship between the aeration efficiency and energy dissipation rate. This procedure could have practical implications for predicting hydraulic jump aeration efficiency.

Pagliara *et al.* (2010.) described the free surface flow over a rough bed at steep slopes entrains large amounts of air bubbles due to the high interaction between the free surface and the bed materials. The assessment of mixed air-water flow features in the presence of a three-dimensional bed configuration from macro roughness to intermediate roughness conditions can hardly be accomplished with aeration models developed for smooth or stepped bed configurations. Two-phase flow properties were measured over rough bed materials in a setup assembled at the PITLAB centre at the University of Pisa, Italy. Coarser protruding materials were incorporated over the rough bed to intensify the aeration in the mixed air-water flow. Flow discharges ranging between 0.02 and 0.09 m^3/s and slopes between 0.18 and 0.44 were tested. A detailed study of the air-water inner layer and flow features over staggered and row coarser material arrangement over the base material was carried out. Results were compared with literature data on free-surface flow over smooth and stepped beds.

Tammela *et al.* (2010) used the wooden debris structures, commonly used in stream restoration to alter sediment transport and flow distributions, to improve fish habitats in degraded streams. Various wooden structures were tested in a laboratory flume to determine their ability to change flow patterns, resulting in local scour. A parametric study was made to predict scour hole depth. The results indicated that the under-miner structure should cover the full channel width and divert the whole flow below the structure. Maximum scour depth was obtained with a single structure perpendicular to the flow direction and overall scour depth was governed by structural height and sediment particle size distribution. With increasing structure angle with respect to flow, the area and volume of the scour hole increase, whereas the scouring depth decreases. Coarser sediment size reduces scour depth for both single and consecutive structures. The optimum under miner spacing ratio was found to be 2 to 3 times the channel width.

Bostan *et al.* (2013) described one of the most important parameters to determine the quality of water as the amount of dissolved oxygen (DO) in the water body. Microorganisms such as bacteria need a high concentration of oxygen in the water to the ability to continue their lives healthfully. In this case, the concentration of the DO in the water body should be greater than 5 mg/l. The hydraulic jump is used as an effective natural mechanic mixer for the oxygen transfer from air to the water body. This study aimed to investigate the aeration efficiency created by the water jet vertically on the turbulence shear layer in the hydraulic

jump. The experiments were realized in an open channel having a width of 0.4 meters, a height of 0.65 meters and a length of 12 meters. The DO was measured using a DO200 hand-type oxygen meter. Experiments were taken into account five different jet flow rates and Froude numbers (*Fr*) within the range of 3.55 to 6.07.

Raikar and Kamatagi (2015) pointed out that the DO content in water bodies is an indicator of water quality and hence a measure of the ability of water to sustain aquatic life. Hydraulic phenomena such as hydraulic drops and hydraulic jumps can increase the amount of DO in the water by creating turbulent conditions. The main reason for this oxygen transfer is the air entrainment into the flow through a large number of air bubbles that helps in air-water transfer. This study investigated the effect of different weir types and hydraulic jumps on their aeration efficiency. Two types of weirs namely rectangular and triangular weirs were used. Also, the hydraulic jump was studied as an aeration agent. From the experimental results, it was found that the triangular weir provides greater aeration efficiency of 0.1948 as compared with the rectangular weir which had an aeration efficiency of 0.1012. On the other hand, the hydraulic jump showed an aeration efficiency of 0.14285. As the weirs are more efficient than hydraulic jump, they are most applicable in the field. Also, weir structures are less expensive when compared with the structural arrangement required for the formation of hydraulic jump.

Kim *et al.* (2016) examined the oxygen transfer and the energy dissipation by the flow types at the stepped weir structure performed through hydraulic experiments. Nappe flow occurs at low flow rates and for a relatively small step slope. Dominant features of an air pocket, nappe impact and subsequent hydraulic jump occur. At larger flow rates, skimming flow occurs with the formation of re-circulating vortices. Transition flow showed the simultaneous occurrence of skimming flow at upper steps and nappe flow at lower steps. Air entrainment occurs through free-falling nappe impact and subsequent hydraulic jump in the nappe flow, and occurs from the step edges in the skimming flow. Energy dissipation occurs through the jet impact and the subsequent hydraulic jump in the nappe flow and occurs through maintaining the recirculation vortices between step edges in the skimming flow regimes. The average values of the oxygen transfer are 0.45 in the nappe flow and 0.28 in the skimming flow, and the efficiencies of energy dissipation in the nappe flow and the skimming flow are about 70~95(%) and 60~90(%), respectively. From these results, the stepped weir structure was found to be efficient for oxygen transfer and energy dissipation.

Eltoukhy (2016) examined that the hydraulic jump can be considered the best way for dissipating energy present in moving water downstream of hydraulic structures. This paper conducted laboratory experiments to investigate the hydraulic jump characteristics variations for different rectangular open channel layouts with five bed slopes of 0.0175, 0.0349, 0.0524, 0.0699, and 0.0875, and a sill with three different heights was placed along a model of the stilling basin at three different longitudinal distances. The characteristics of the hydraulic jump, which was formed downstream vertical gate, were measured for variable discharges. Results of experiments show that the hydraulic jump ratios, jump length and initial depth ratio, Lj/y_1, jump length and sequent depth ratio, Lj/y_2, jump depths ratio, y_2/y_1, y_2-y_1, and relative energy loss and initial energy ratio, D_E/E_1 increase with initial Froude's number for different bed slopes. On the other hand, results show that the sill has a significant effect on energy dissipation. A new equation was developed to design stilling basin, i.e., the sill height, *H*, and the longitudinal distance, *L*.

Jaiswal and Goel (2019) performed that aeration is a process, which helps in the enhancement of the concentration of dissolved oxygen in the water. The concentration of DO is required for sustaining aquatic life and is also considered an indicator of the quality of water. The DO can be enhanced by using either a mechanical aerator or hydraulic structures. Hydraulic structures accelerate the water–air–mass transfer by entraining a large amount of air in the form of a bubble, thus increasing the surface contact area for full oxygen transfer. Commonly hydraulic structures used for aeration are weirs, spillways, cascades, water jets and close conduit flow arrangements, etc. When the performance of weirs is compared with other aerating agents like hydraulic jump, labyrinth weirs, chutes etc., it was found that weirs give maximum oxygen transfer efficiency. From previous literatures, they used data on rectangular, triangular, trapezoidal and semi-circular shaped weirs for DO studies. They looked into the literature review of weirs having free surfaces when employed for aeration purposes for wastewater treatment. It was found that the triangular-shaped weir has created maximum oxygen transfer efficiency out of all other shapes of the weir. It was expected that the findings of this study may help in the selection of particular weir configurations and shapes of weir for creating maximum oxygen transfer efficiency in the rivers and streams for the treatment of water.

Hoque and Paul (2022) analysed the different similarities of air entrainment among the hydraulic jumps, plunging jets, and plunging breaking waves to discuss the practices during that period. The measured data were re-examined and scrutinised to investigate the gas exchange phenomena through an air-water interface. In particular, oxygen transfer efficiency and penetration depth by air bubbles were discussed. The calculated results highlight that the oxygen transfer efficiency is decreased with the increase of energy dissipation rate both in plunging jets and breaking waves. In contrast, it was shifted almost parallel in the case of hydraulic jumps. In addition, the aeration lengths in the hydraulic jumps and penetration depths both in plunging jets and plunging breaking waves were dependent on the jet impact velocity.

Bai *et al.* (2022) examined that the hydraulic jump may form when a supercritical flow runs over a vegetated bottom and change the downstream flow hydraulics and fluid properties after air-water mixing and energy dissipation at the flow transition. Unlike the abundant literature on hydraulic jump characteristics on engineered or natural sediment trough beds, few studies of vegetation roughness effects have been reported. New experiments were conducted by creating hydraulic jumps with identical inflow Froude numbers on a smooth bed, fully and partly grated rough beds, and partially vegetated grate rough beds covered with artificial plants of different densities. The free-surface dynamics and air-water flow properties were investigated with a primary focus on the interaction between the flow and flexible vegetation barrier/roughness, in addition to the effects of Froude number and inflow roughness conditions. The characteristic jump and jump roller lengths were found shortened as the jump roller was deflected over the vegetation layer. The flow structure modification was observed with a steepening of the roller free-surface profile and enhanced surface wave propagation, especially when the flow experienced an invert roughness discontinuity at the toe. An increasing bubble detection frequency was obtained in non-vegetated channels when the bed was roughened, but additional vegetation on the rough invert caused a reduction in the bubble frequency and cross-sectional mean air concentration by inducing roller deflection and air bubble detrainment. The results indicated that the effects of perturbing artificial flexible vegetation with relatively large plant height could be different from uniformly

distributed rigid bed roughness elements and computed by the time-varying flow vegetation interaction.

From the above-mentioned literature, it is very much clear that several studies on hydraulic jumps have been carried out. Most of them were mainly about the hydraulic jump, aeration, entrainment of air into the flow, aeration efficiency, energy losses, slope variation, and dissolved oxygen.

In the present study, an attempt has been made with a rectangular tilting flume to find out the variation of dissolved oxygen at different ambient temperatures, slopes, and hydraulic jumps and also to find out the energy losses due to the hydraulic jump.

CHAPTER 3

3.1 Rapidly Varied Flow for Hydraulic Jump

3.1.1. The Momentum Equation

The definition sketch of a hydraulic jump in a prismatic channel of arbitrary shape is presented in Fig. 3.1. The channel is inclined to the horizontal at an angle θ. Sections 1 and 2 refer to the beginning and end of the jump respectively.

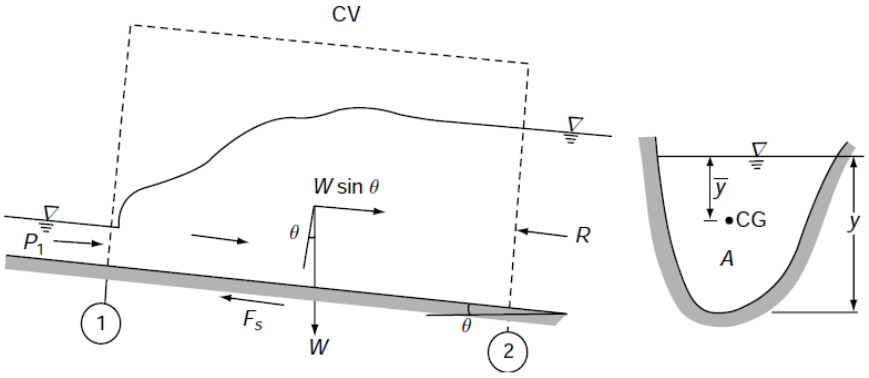

Fig. 3.1 Definition sketch for the general momentum equation.

A control volume (CV) enclosing the jump as shown by dashed lines in Fig. 3.1, is selected. The flow is considered to be steady. Applying the linear momentum equation in the longitudinal direction to the control volume,

$$P_1 - P_2 - F_s + \mathrm{W}\,\mathbf{sin}\;\theta \;=\; \mathrm{M}_2 - \mathrm{M}_1 \qquad (3.1)$$

where

P_1 = pressure force at the control surface at Section 1=$\gamma\, A_1\bar{y}_1\cos\theta$ by assuming hydrostatic pressure distribution, where y_1 = depth of the centroid of the area below the water surface.

P_2 = pressure force at the control surface at Section 2= $\gamma\, A_2\bar{y}_2\cos\theta$ if hydrostatic pressure distribution is assumed. (Note that $P \approx \gamma\, \bar{y}\, A$ if θ is small.)

Fs = shear force on the control surface adjacent to the channel boundary.

W sin θ = longitudinal component of the weight of water contained in the control volume.

M_2 = momentum flux in the longitudinal direction going out through the control surface = $\beta_2 \rho Q V_2$.

M_1 = momentum flux in the longitudinal direction going in through the control surface = $\beta_1 \rho Q V_1$.

The hydraulic jump is a rapidly-varied flow phenomenon and the length of the jump is relatively small compared to GVF profiles. Thus, frictional force F_s is usually neglected as it is of secondary importance. Alternatively, for smaller values of θ, ($W\sin\theta - F_s$) can be considered to be very small and hence are neglected. For a horizontal channel, $\theta = 0$ and $W \sin\theta = 0$.

3.2 Hydraulic Jump in a Horizontal Rectangular Channel

3.2.1. Sequent Depth Ratio

Consider a horizontal, frictionless and rectangular channel. Considering the unit width of the channel, the momentum equation, Eq. 3.1. can be written in the form

$$\frac{1}{2}\gamma y_1^2 - \frac{1}{2}\gamma y_2^2 = \beta_2 \rho q V_2 - \beta_1 \rho q V_1 \tag{3.2}$$

Taking, $\beta_1 = \beta_2 = 1.0$ and noting that by continuity
q= discharge per unit width = $V_1 y_1 = V_2 y_2$

$$y_2^2 - y_1^2 = \frac{2q^2}{g}\left(\frac{1}{y_1} - \frac{1}{y_2}\right), \tag{3.3}$$

$$y_1 y_2 \left(y_1 + y_2\right) = \frac{2q^2}{g} = 2y^3{}_c \tag{3.4}$$

$$\frac{1}{2}\left(\frac{y_2}{y_1}\right)\left(1 + \frac{y_2}{y_1}\right) = \frac{q^2}{g y^3{}_1} = F_1^2 \tag{3.5}$$

where F_1 =Froude Number of the approach flow = $V_1/\sqrt{g y_1}$
Solving for y_2/y_1 yields

$$\frac{y_2}{y_1} = \frac{1}{2}\left[-1 + \sqrt{1 + 8F_1^2}\right] \tag{3.6}$$

This equation which relates the ratio of the sequent depths (y_2 / y_1) to the initial Froude number F_1 in a horizontal, frictionless, rectangular channel is known as the Belanger momentum equation. For high values of F_1, say $F_1 > 8.0$, can be approximated for purposes of quick estimation of the sequent depth ratio as $y_2 / y_1 \approx 1.41$
$F_2 = V_2(g y_2)^{0.5}$= subcritical Froude number on the downstream of the jump as-

$$\frac{y_1}{y_2} = \frac{1}{2}\left(-1 + \sqrt{1 + 8F^2{}_2}\right) \tag{3.7}$$

3.2.2. Energy Loss

The energy loss E_L in the jump is obtained by the energy equation applied to Sections 1 and 2 as

$$E_L = E_1 - E_2 = \left(y_1 - y_2\right) + \frac{1}{2}\frac{q^2}{g}\left(\frac{y_2^2 - y_1^2}{y_1^2 y_2^2}\right) \tag{3.8}$$

After simplifying

$$E_L = \frac{\left(y_2 - y_1\right)^3}{4 y_1 y_2} \tag{3.9}$$

or
$$\frac{E_L}{y_1} = \frac{\left(\frac{y_2}{y_1} - 1\right)^3}{4\left(\frac{y_2}{y_1}\right)} \tag{3.10}$$

After calculating

$$\frac{E_L}{E_1} = \frac{\left(-3 + \sqrt{1 + 8F_1^2}\right)^3}{8\left(2 + F_1^2\right)\left(-1 + \sqrt{1 + 8F_1^2}\right)} \tag{3.11}$$

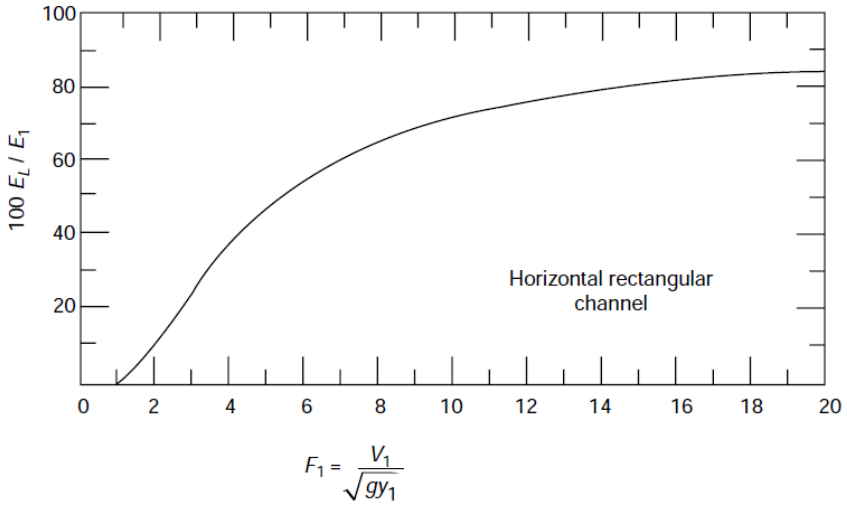

Fig. 3.2 Relative energy loss in a jump.

3.2.3. Classification of Jumps

As a result of extensive studies by Bradley and Peterka (1957) the hydraulic jumps in horizontal rectangular channels are classified into five categories based on the Froude number F_1 of the supercritical flow, as follows:

(i) Undular Jump $1.0 < F_1 \leq 1.7$ The water surface is undulating with a very small ripple on the surface. The sequent-depth ratio is very small and E_L/E_1 is practically zero. A typical undular jump is shown in Fig. 3.3.

(ii) Weak Jump $1.7 < F_1 \leq 2.5$ The surface roller makes its appearance at $F_1 \approx 1.7$ and gradually increases in intensity towards the end of this range, i.e., $F_1 \approx 2.5$. The energy dissipation is very small, is E_L/ E_1 about 5% at $F_1 = 1.7$ and 18% at $F_1 = 2.5$. The water surface is smooth after the jump Fig. 3.4.

(iii) Oscillating Jump $2.5 < F_1 \leq 4.5$ This category of the jump is characterised by an instability of the high-velocity flow in the jump which oscillates in a random manner between the bed and the surface. These oscillations produce large surface waves that travel considerable distances downstream. A typical oscillating jump is shown in Fig. 3.5.

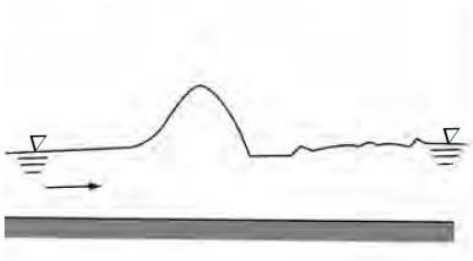

Fig. 3.3 Undular Jump 1.0< $F_1 \leq 1.7$

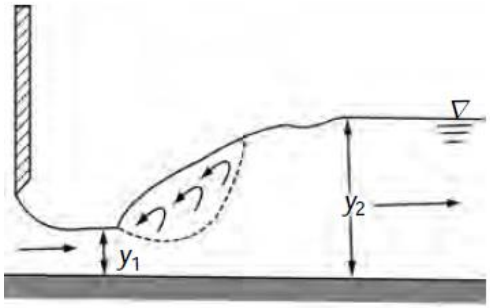

Fig. 3.4 Weak jump 1.7< $F_1 \leq 2.5$

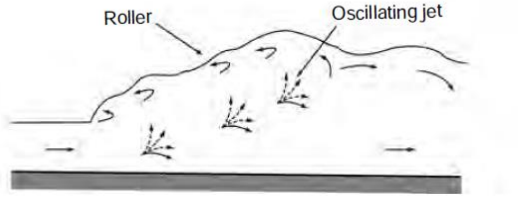

Fig. 3.5 Oscillating jump 2.5< $F_1 \leq 4.5$

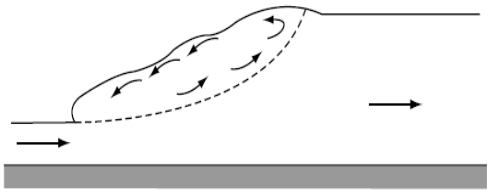

Fig. 3.6 Steady jump 4.5 < $F_1 \leq 9.0$

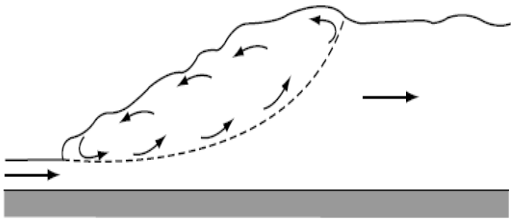

Fig. 3.7 Strong jump F_1> 9.0

Special care is needed to suppress the waves in stilling basins having this kind of jump. Energy dissipation is moderate in this range; E_L / E_1 = 45% at F_1 = 4.5.

(iv) Steady Jump 4.5 < $F_1 \leq 9.0$ In this range of Froude numbers, the jump is well-established, and the roller and jump action is fully developed to cause appreciable energy loss Fig. 3.6. The relative energy loss E_L / E_1 ranges from 45% to 70% in this, class of jump. The 'steady jump' is least sensitive in terms of the toe position to small fluctuations in the tail-water elevation.

(v) Strong or Choppy Jump $F_1 > 9.0$ In this class of jump the water surface is very rough and choppy. The water surface downstream of the jump is also rough and wavy Fig. 3.7. The sequent-depth ratio is large and the energy dissipation is very efficient with E_L/E_1 values greater than 70%.

It is of course obvious that the above classification is based on purely subjective consideration of certain gross physical characteristics. As such, the range of Froude numbers indicated must not be taken too rigidly. Local factors in stilling basin design can cause

overlaps in the range of Froude numbers. The figure shows four typical hydraulic jumps in a rectangular laboratory flume.

$$\frac{E_L}{y_1} = \frac{1}{16}\frac{\left(-3+\sqrt{1+8F_1^2}\right)^3}{\left(-1+\sqrt{1+8F_1^2}\right)} \tag{3.12}$$

Since, $F_1^2 = q^2/gy^3_1$, $y_1 = q^{2/3}/g^{1/3}F_1^{2/3}$

Substituting for y_1 in the expression for E_L/y_1 given above,

$$\frac{16g^{1/3}E_l}{q^{2/3}} = \frac{\left(-3+\sqrt{1+8F_1^2}\right)}{\left(F_1\right)\left(-1+\sqrt{1+8F_1^2}\right)} = f\left(F_1\right) \tag{3.13}$$

A common problem encountered in the hydraulic design of stilling basins for barrages is estimating the elements of the hydraulic jump when discharge intensity (q) and energy loss (E_L) are the only known parameters of the jump. Equation 3.13 is a very useful context. A trial-and-error solution procedure is used to solve Eq. 3.13 to obtain F_1 for known q and E_L. Knowing F_1, other parameters of the jump are then found by direct use of the relevant equations.

3.2.4. Characteristics of Jump in a Rectangular Channel

(i) Length of the Jump

The length of the jump L_j is an important parameter affecting the size of a stilling basin in which the jump is used. There have been many definitions of the length of the jump resulting in some confusion in comparing various studies. It is now usual to take the length of the jump as the horizontal distance between the toe of the jump to a section where the water surface levels off after reaching the maximum depth (Fig. 1.1). Because the water-surface profile is very flat towards the end of the jump, large personal errors are introduced in the determination of the length L_j.

Experimentally, it is found that $Lj / y_2 = f(F_1)$. The variation of L_j/y_2 with F_1 obtained by Bradley and Peterika (1957) is shown in Fig. 3.8. This curve is usually recommended for general use. It is evident from Fig. 1.1. that while Lj/y_2 depends on F_1 for small values of the inlet Froude number, at higher values (i.e., $F_1 > 5.0$) the relative jump length L_j/y_2 is practically constant beyond a Froude number value of 6.1. Elevatorski (1959) showed that the data of jump length can be expressed a

$$Lj = 6.9(y_2 - y_1) \tag{3.14}$$

(ii)Pressure Distribution

The pressures at the toe of the jump and the end of the jump follow hydrostatic pressure distribution. However, inside the body of the jump, the strong curvatures of the streamlines cause the pressures to deviate from the hydrostatic distribution. Observations by Rajaratnam

(1967) have shown that in the initial portions of the jump the pressures in the jump body will be less than the hydrostatic pressure. The deficit from the hydrostatic pressure increases with an increase in the initial Froude number F_1. However, at the bottom of the channel and in a narrow region close to the bed, the pressures are essentially hydrostatic. Thus, the pressure-head profile on the bed is the same as the mean water-surface profile.

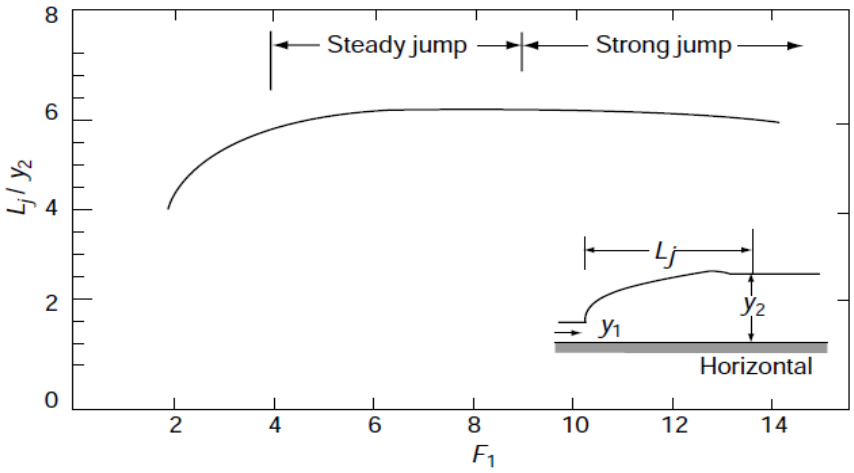

Fig. 3.8 Length of the hydraulic jump on a horizontal floor.

(iii)Water-Surface Profile

Knowledge of the surface profile of the jump is useful in the efficient design of side walls and the floor of a stilling basin. Consider the coordinate system shown in Fig. 3.9. The coordinates of the profile are (x, h) with the boundary condition that at $x = 0$, $h = 0$, and at $x = Lj$, $h = (y_2 - y_1)$. In general, $h = f(x, F_1)$. Based on an analysis of a large number of jump profiles and bed-pressure profiles obtained by various investigators, Subramanya and Rajaratnam and Subramanya (1968) have shown that the jump profile can be expressed in a non-dimensional manner as

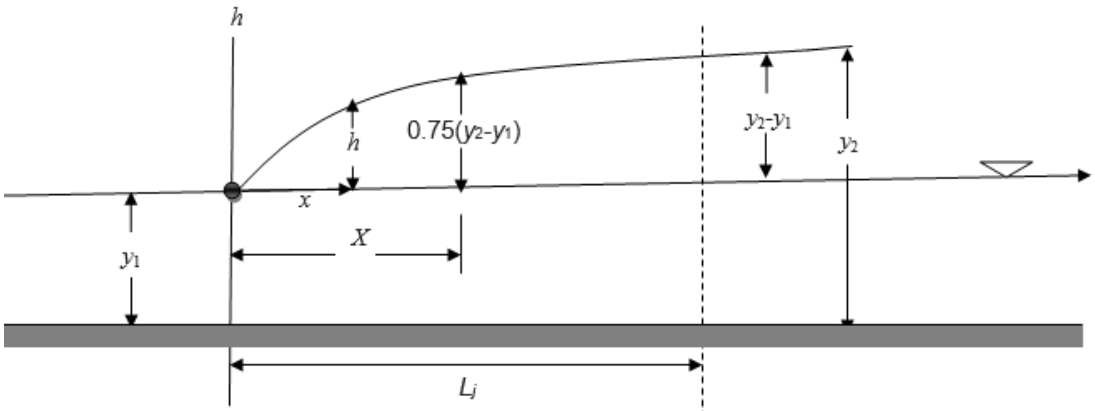

Fig. 3.9 Definition sketch for the jump profile.

(iv)Velocity profile

When the supercritical stream at the toe enters the jump body, it undergoes shearing action at the top as well as at the solid boundaries. The top surface of the high-velocity flow will have

high relative velocities with respect to the fluid mass that overlays it. The intense shear at the surface generates a free shear layer which entrains the fluid from the overlying mass of fluid. The boundary shear at the bed causes retardation of the velocity in a boundary layer. As a result of these actions, the velocity distribution in a section at a distance x from the toe will be as shown in Fig. 3.10. It is seen that the velocity profile has two distinct portions—a forward flow in the lower main body and a negative velocity region at the top. In the forward flow, the total volumetric rate of flow will be in excess of the discharge Q entering the jump at the toe. This is due to the flow entrainment at the shear layer. To maintain continuity, i.e., to account for the excess forward flow, a reverse flow exists at the top. This situation results in the formation of the roller.

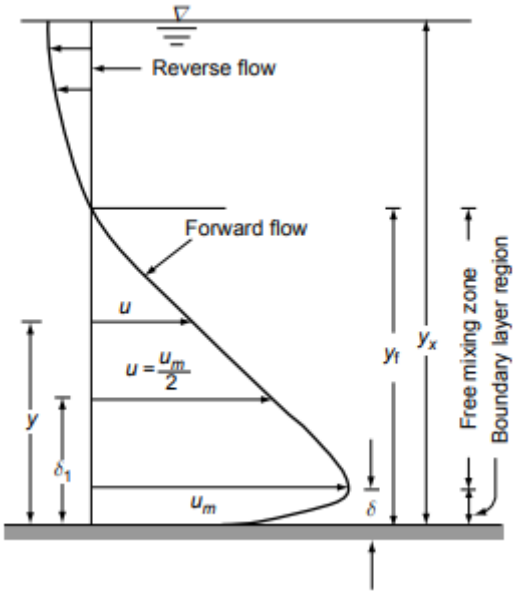

Fig. 3.10 Velocity distribution in a jump

The forward velocity profile has zero velocity at the bed, the maximum velocity at a distance δ and then gradually decreases to zero at a height y_f above the bed. The region $0 < y < \delta$ can be called the boundary layer part and the region $\delta < y < y_{f\,is}$ the free-mixing zone. This velocity configuration indicates that the motion of the forward flow is similar to a wall jet except that the pressure gradient is adverse. The velocity profile and shear stress can be studied by following methods of analysis similar to those used in the study of wall jets.

The velocity u at a distance y from the bed in the boundary layer portion ($0 < y < \delta$) can be expressed by a velocity-defect law

$$\frac{u - u_m}{u_*} = f\left(\frac{y}{\delta}\right) \tag{3.15}$$

where $u_* = \sqrt{T_0/\rho}$= shear velocity and u_m = maximum velocity at $y = \delta$. In the free mixing zone, the velocity profile is found to be self-similar and can be expressed as

$$\frac{u}{u_m} = f\left(\frac{y}{\delta_1}\right) \quad \text{for } y/\delta_1 > 0.16 \tag{3.16}$$

where δ_1 =value of y at which. $u = u_m/2$ The maximum velocity um occurs at $y=\delta \approx 0.16\delta_1$. It may be noted that the non-dimensionalised velocity profile is explicitly independent of F_1 and x. The scales of the above relationship are um and δ_1 which are given by

$$\frac{u_m}{y_1} = f\left(\frac{x}{y_1}\right) \tag{3.17}$$

and

$$\frac{\delta_1}{y_1} = f\left(\frac{x}{y_1}\right) \tag{3.18}$$

Both Eq. 3.17 and Eq. 3.18 are found to be independent of the initial Froude number F_1.

(v) **Other Characteristics**

In addition to the characteristics mentioned above, information about shear stress and turbulent characteristics enhances one's understanding of the jump phenomenon. It has been found that the initial boundary-layer thickness and the relative roughness of the bed play a major role in these aspects. Useful information on these topics is available in the literature.

(vi) Computations

Computations related to hydraulic jumps in rectangular channels are relatively simple. While most of the problem types are amenable to direct solution, a few types require trial and error solution procedure. The available relations are

1. Continuity equation
2. Momentum equation for sequent depths and
3. Energy equation for energy loss in the jump. The basic variables can be discharge intensity q; sequent depths y_1 and y_2; and energy loss E_L. There can be many other derived variables and corresponding relationships. Based on the above there can be a variety of problem types and a few common ones are illustrated in the following examples.

3.3. Jumps on a Sloping Floor.

When a hydraulic jump occurs in a channel with a sloping floor, the situation is described by the general momentum equation, Eq. 3.1. There are too many unknown terms relative to the number of available equations and unless additional information is provided the solution of the momentum equation is not possible. Even if the simplified situation of a rectangular frictionless channel is considered, the term $W\sin\theta$ representing the longitudinal component of the weight of the water in the jump poses a problem as an unknown quantity. This is because $W\sin\theta$ involves the length and profile of the jump, information about which can be obtained only through experimental observations. As such, even though many attempts have been made to obtain the sequent-depth ratio through the momentum equation, no satisfactory general solution is available so far. An example of a typical simplification of Eq.3.1. to obtain

the sequent-depth ratio in a jump on a sloping floor is given below. The definition sketch of a jump on a sloping floor in a rectangular frictionless channel is indicated in Fig. 3.11. The momentum correction factors β_1 and β_2 are assumed equal to unity. A unit width of the channel is considered with q = discharge per unit width, y_1 = depth before the jump and y_t = depth at the end of the jump. Consider a control volume as shown by dashed lines and the momentum equation in the longitudinal direction would be, from Eq. 3.1.

$$P_1 - P_2 + W\sin\theta = M_2 - M_1 \tag{3.19}$$

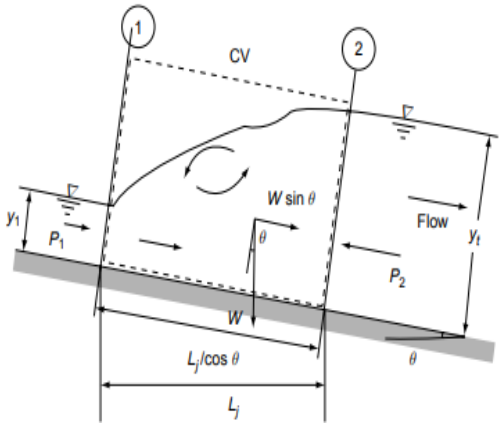

Fig. 3.11 Definition sketch for a jump on a sloping floor.

Assuming hydrostatic pressure distribution in Sections 1 and 2,

$$P_1 = 1/2\gamma y^2_1 \cos\theta$$

$$P_2 = 1/2\gamma y^2_2 \cos\theta$$

If the water surface were a straight line joining y_1 and y_t then the area of the jump $=1/2(y_1+y_t)\, Lj/\cos\theta$.

Note that the length of the jump Lj is defined as a horizontal distance between y_1 and y_t. Introducing a coefficient to account for the curvature of the jump profile and $\cos\theta$ term,

$$W = \frac{1}{2} K\gamma L_j \left(y_1 + y_t\right) \tag{3.20}$$

The momentum flux $M_1 = \rho q^2/y_1$ and $M_2 = \rho q^2/y_t$
Equation 3.19. can now be re-written as

$$\frac{1}{2}\gamma\left(y_1^2\cos\theta - y_t^2\cos\theta + KL_j\left(y_1 + y_2\right)\sin\theta\right) = \rho q^2\left(\frac{1}{y_t} - \frac{1}{y_1}\right) \tag{3.21}$$

where $F_1 = V_1/\sqrt{g y_1}$

Note that F_1 is not the exact Froude number of the inclined channel flow at Section 1= F_{1s} but is only a convenient non-dimensional parameter. The Froude number of flow in channels with large θ is given. Hence for α =1.0, $F_{1s} = V_1\sqrt{g(A/T)}\cos\theta$
i.e.,

$$\left(\frac{y_t}{y_1}\right)^3 - \frac{KL_j \tan\theta}{y_t}\left(\frac{y_t}{y_1}\right)^2 - \left(1 + \frac{KL_j \tan\theta}{y_1} + \frac{2F_1^2}{\cos\theta}\right)\left(\frac{y_t}{y_1}\right) + \frac{2F_1^2}{\cos\theta} = 0 \qquad (3.22)$$

Equation 3.22 can be used to estimate the sequent-depth ratio by a trial-and-error procedure if the term *(KLj)* is known. In general, (*KLj*) can be expected to be a function of F_1 and θ and its variation can be obtained only through experimental study.

3.3.1 Characteristics of Jumps on a Sloping Floor

Extensive experiments have been conducted by the U.S. Bureau of Reclamation resulting in useful information on jumps on a sloping floor. Based on the USBR study, the following significant characteristics of sloping-floor jumps can be noted.

i) **Sequent Depth y_t**

Defining y_2 = equivalent depth corresponding to y_1 in a horizontal floor jump = $(1/2)\, y_1(-1+\sqrt{(1+8F_1^2)})$, the sequent depth y_t is found to be related to y_2 as`

$$y_t/y_2 = f(\theta)$$

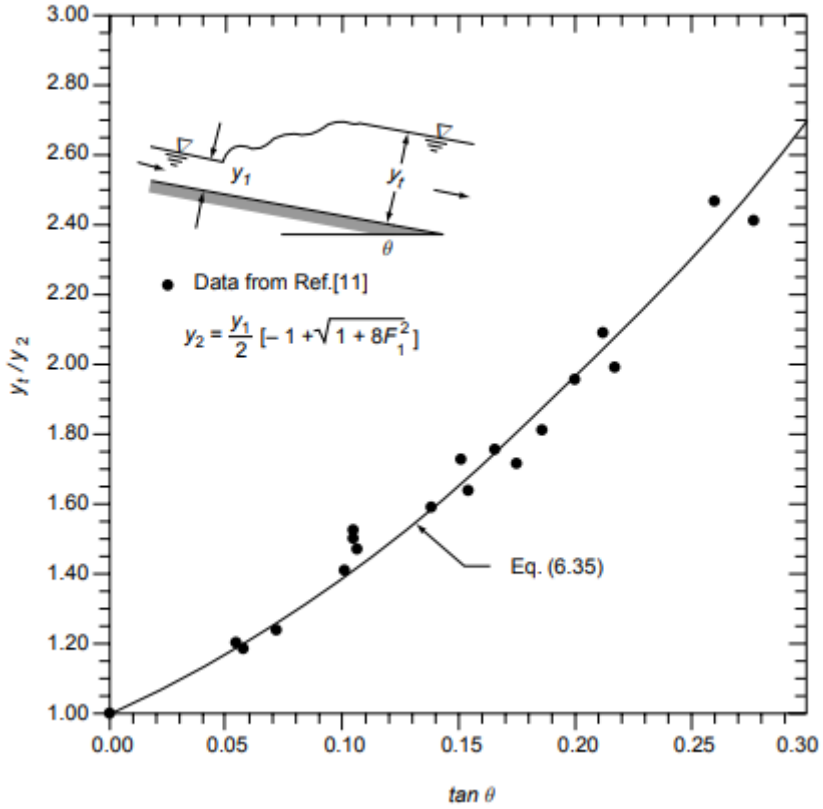

Fig. 3.12 Variation of y_t/y_1 in jumps on a sloping floor.

The variation of (y_t/y_1) with tan θ is shown in Fig. below. By definition $y_t/y_2 = 1.0$ when tan $\theta = 0$ and it is seen from Fig. top that y_t/y_2 increases with the slope of the channel having typical values of 1.4 and 2.7 at tan θ = 0.10 and 0.30 respectively. Thus, the sloping-floor jumps require more tailwater depths than the corresponding horizontal-floor jumps.

The best fit line for the variation of y_t/y_2 with tan θ shown in Fig. 3.12 can be expressed as

$$y_t / y_2 = 1.0071 \times exp\left(3.2386 \times tan\theta\right) \tag{3.23}$$

ii) Length of the Jump *L*j

The length of the jump *L*j was defined in the USBR study as the horizontal distance between the commencement of the jump and a point on the subcritical flow region where the streamlines separate from the floor or to a point on the level water surface immediately downstream of the roller, whichever is longer.

The length of the jump on a sloping floor is longer than the corresponding *Lj* of a jump on a horizontal floor. The variation of *L*j / y_2 with F_1 for any θ is similar to the variation for $\theta = 0$ case shown in Fig.3.8. In the range of $4.0 < F_1 < 13$, *L*j / y_2 is essentially independent of F_1 and is a function of θ only. The variation can be approximately expressed as

$$\frac{L_j}{y_2} = 6.1 + 4.0 \tan\theta \tag{3.24}$$

In the range of $4.5 < F_1 < 13.0$

Elevatorski's (1959) analysis of the USBR data indicates that the jump length can be expressed as

$$L_j = m_s (y_t - y_1) \tag{3.25}$$

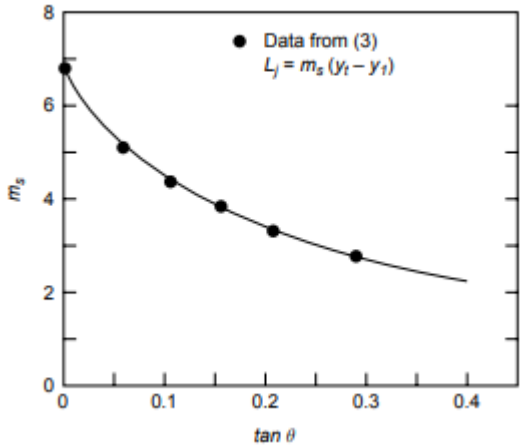

Fig. 3.13 Length of jumps on the sloping floor

In which $m_s = f(\theta)$. The variation of ms with tan θ is shown in Fig. 3.13 It may be seen that m_s = 6.9 for tan $\theta = 0$ and decreases with an increase in the value of the channel slope. Equation 3.25. is based on a wider range of values for F_1 than in Eq. 3.25.

iii) Energy Loss E_L

Knowing the sequent depths y_t and y_1 and the length of the jump, the energy loss E_L can be calculated as $E_L = H_1 - H_2$ where H = total energy at a section

$$E_L = (E_1 + L_j \tan\theta) - E_2 = y_t \cos\theta + \frac{V_t^2}{2g} + L_j \tan\theta - y_t \cos\theta - \frac{V_1^2}{2g} \qquad (3.26)$$

where y_t = sequent depth in a sloping channel at Section 2. It is found that the relative energy loss E_L/H_1 decreases with an increase in the value of θ, being highest at tan θ = 0. The absolute value of E_L is a function of θ, being least when $\theta = 0$.

CHAPTER 4

4.1. Dissolved Oxygen

Dissolved oxygen refers to the level of free, non-compound oxygen present in water or other liquids. It is an important parameter in assessing water quality because of its influence on the organisms living within a body of water. In limnology (the study of lakes), dissolved oxygen is an essential factor second only to water itself. A dissolved oxygen level that is too high or too low can harm aquatic life and affect water quality. Figure 4.1. shows the dissolved oxygen in the water.

Non-compound oxygen or free oxygen (O_2) is oxygen that is not bonded to any other element. Dissolved oxygen is the presence of these free O_2 molecules within the water. The bonded oxygen molecule in water (H_2O) is in a compound and does not count toward dissolved oxygen levels. One can imagine that free oxygen molecules dissolve in water much the way salt or sugar does when it is stirred.

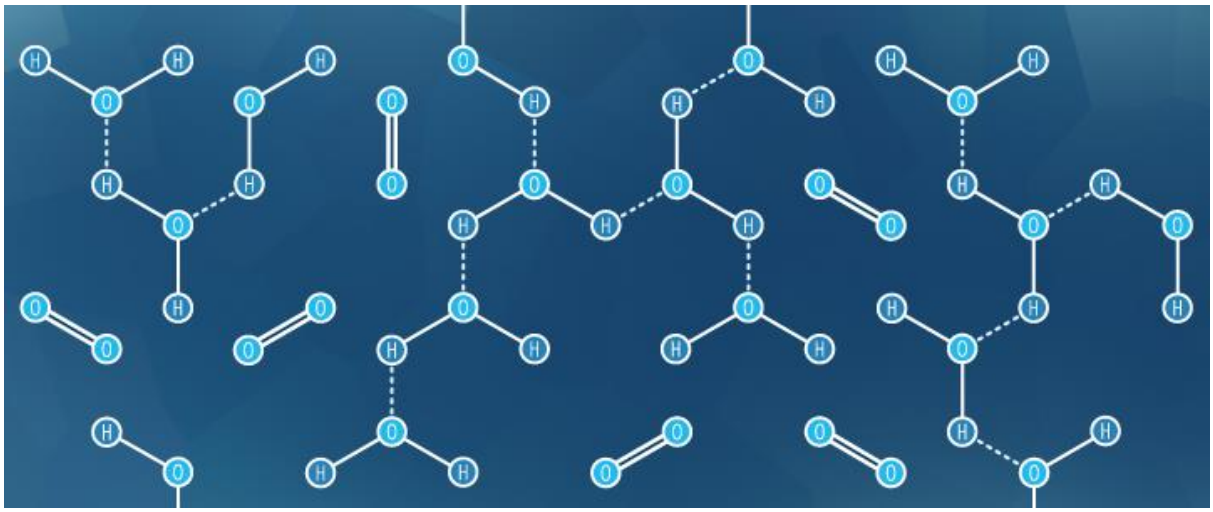

Fig. 4.1 Dissolved oxygen in the water.

4.2. Dissolved Oxygen and Aquatic Life

Dissolved oxygen is necessary for many forms of life including fish, invertebrates, bacteria and plants. These organisms use oxygen in respiration, similar to organisms on land. Fish and crustaceans obtain oxygen for respiration through their gills, while plant life and phytoplankton require dissolved oxygen for respiration when there is no light for photosynthesis. The amount of dissolved oxygen needed varies from creature to creature. Bottom feeders, crabs, oysters and worms need minimal amounts of oxygen (1-6 mg/l), while shallow water fish need higher levels (4-15 mg/l). Figure 4.2. shows that DO is important to many forms of aquatic life.

Microbes such as bacteria and fungi also require dissolved oxygen. These organisms use DO decompose organic material at the bottom of a body of water. Microbial decomposition is an important contributor to nutrient recycling. However, if there is an excess of decaying organic material (from dying algae and other organisms), in a body of water with infrequent or no turnover (also known as stratification), the oxygen at lower water levels will get used up quicker.

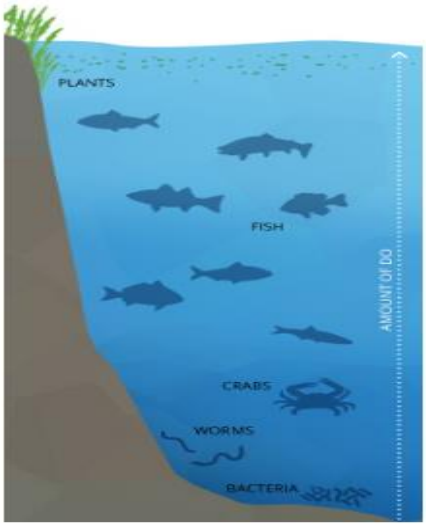

Fig. 4.2 Dissolved oxygen is important to many forms of aquatic life.

4.3. Sources of DO

Dissolved oxygen enters the water through the air or as a plant by-product. From the air, oxygen can slowly diffuse across the water's surface from the surrounding atmosphere, or be mixed in quickly through aeration, whether natural or man-made. The aeration of water can be caused by wind (creating waves), rapids, waterfalls, groundwater discharge or other forms of running water. Man-made causes of aeration vary from an aquarium air pump to a hand-turned waterwheel to a large dam. Dissolved oxygen is also produced as a waste product of photosynthesis for phytoplankton, algae, seaweed and other aquatic plants. Figure 4.3. shows that dissolved oxygen entered the water.

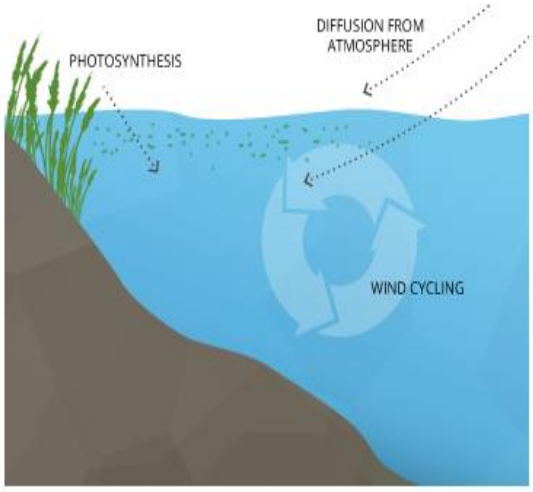

Fig. 4.3. Dissolved oxygen enters the water.

4.4. Dissolved oxygen from photosynthesis

While most photosynthesis takes place at the surface (by shallow water plants and algae), a large portion of the process takes place underwater (by seaweed, sub-surface algae and phytoplankton). Light can penetrate water, though the depth that it can reach varies due to

dissolved solids and other light-scattering elements present in the water. Depth also affects the wavelengths available to plants, with red being absorbed quickly and blue light being visible past 100 m. In clear water, there is no longer enough light for photosynthesis to occur beyond 200 m, and aquatic plants no longer grow. In turbid water, this photic (light-penetrating) zone is often much shallower.

Regardless of the wavelengths available, the cycle does not change. In addition to the needed light, CO_2 is readily absorbed by water (it is about 200 times more soluble than oxygen) and the oxygen produced as a by-product remains dissolved in water. The basic reaction of aquatic photosynthesis remains: $CO_2 + H_2O \rightarrow (CH_2O) + O_2$

As aquatic photosynthesis is light-dependent, the dissolved oxygen produced will peak during daylight hours and decline at night. Figure 4.4. shows that dissolved oxygen can enter the water as a by-product of photosynthesis.

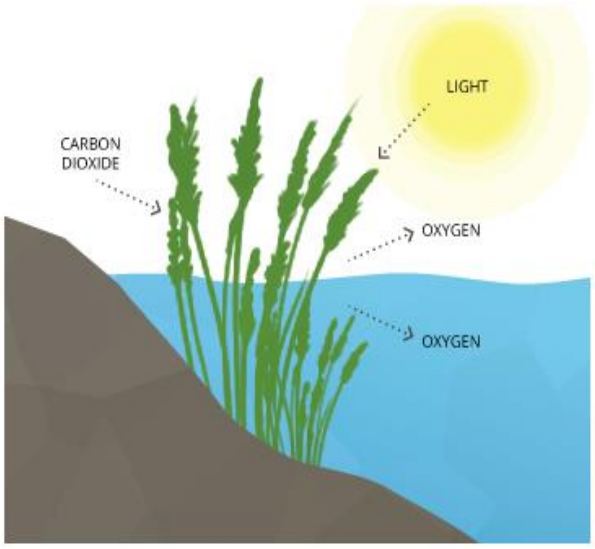

Fig. 4.4 Dissolved oxygen can enter the water as a by-product of photosynthesis

4.5. Dissolved Oxygen Saturation

In a stable body of water with no stratification, dissolved oxygen will remain at 100% air saturation. 100% air saturation means that the water is holding as many dissolved gas molecules as it can in equilibrium. At equilibrium, the percentage of each gas in the water would be equivalent to the percentage of that gas in the atmosphere – i.e. its partial pressure. The water will slowly absorb oxygen and other gasses from the atmosphere until it reaches equilibrium at complete saturation. This process is sped up by wind-driven waves and other sources of aeration.

In deeper waters, DO can remain below 100% due to the respiration of aquatic organisms and microbial decomposition. Figure 4.5. shows these deeper levels of water often do not reach 100% air saturation equilibrium because they are not shallow enough to be affected by the waves and photosynthesis at the surface. This water is below an invisible boundary called the thermocline (the depth at which water temperature begins to decline).

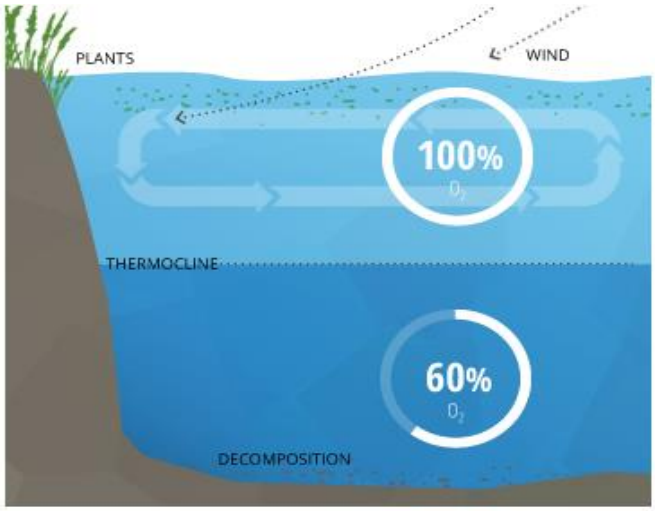

Fig. 4.5 Not all water depths reach 100% air saturation

4.6. Effects of Oxygen Solubility

Two bodies of water that are both 100% air-saturated do not necessarily have the same concentration of dissolved oxygen. The actual amount of DO (in mg/l) will vary depending on temperature, pressure and salinity.

First, the solubility of oxygen decreases as temperature increases. This means that warmer surface water requires less DO to reach 100% air saturation than does deeper, cooler water. For example, at sea level (1 atm or 760 mm Hg) and 4°C (39°F), 100% air-saturated water would hold 10.92 mg/l of dissolved oxygen. But if the temperature were raised to room temperature, 21°C (70°F), there would only be 8.68 mg/l DO at 100% air saturation.

Second dissolved oxygen decreases exponentially as salt levels increase. That is why, at the same pressure and temperature, saltwater holds about 20% less dissolved oxygen than freshwater.

Third, dissolved oxygen will increase as pressure increases. This is true of both atmospheric and hydrostatic pressures. Water at lower altitudes can hold more dissolved oxygen than water at higher altitudes. This relationship also explains the potential for “super saturation” of waters below the thermocline – at greater hydrostatic pressures, water can hold more dissolved oxygen without it escaping. Gas saturation decreases by 10% per meter increase in depth due to hydrostatic pressure. This means that if the concentration of dissolved oxygen is at 100% air saturation at the surface, it would only be at 70% air saturation three meters below the surface.

In summary, colder, deeper fresh waters have the capability to hold higher concentrations of dissolved oxygen, but due to microbial decomposition, lack of atmospheric contact for diffusion and the absence of photosynthesis, actual DO levels are often far below 100% saturation. Warm, shallow saltwater reaches 100% air saturation at a lower concentration, but can often achieve levels over 100% due to photosynthesis and aeration. Shallow waters also remain closer to 100% saturation due to atmospheric contact and constant diffusion.

If there is a significant occurrence of photosynthesis or a rapid temperature change, the water can achieve DO levels over 100% air saturation. At these levels, the dissolved oxygen will dissipate into the surrounding water and air until it levels out at 100%. Figure 4.6. shows changes in DO concentrations with respect to temperature and Fig. 4.7. shows the variation of DO concentrations with changing altitude.

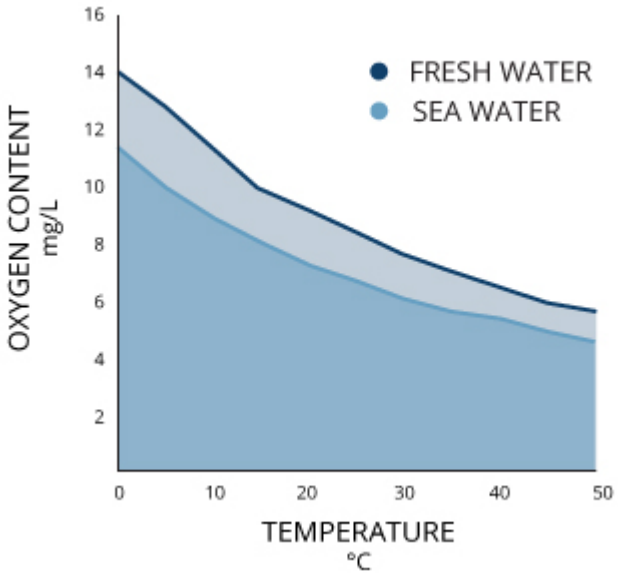

Fig. 4.6 Change of DO concentrations with respect to temperature.

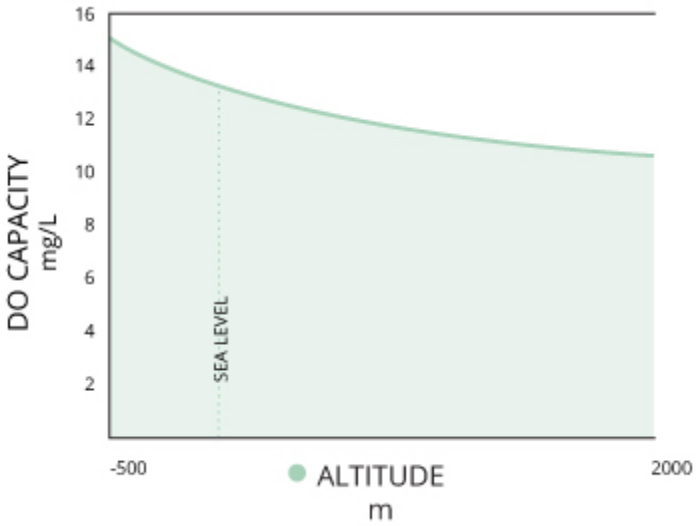

Fig. 4.7 Variation of DO concentrations with changing altitude.

4.7. Self-Aeration Process

In hydraulic jumps and plunging jets, highly turbulent flow and strong mixing structures generate an air-water interface, which ensures gas transfer Kucukali and Cokgor (2006). The term self-aeration means the transfer of oxygen from the air towards the water across a free surface and it has important environmental and ecological implications for polluted streams which have low dissolved oxygen DO levels Kucukali (2005). Aeration efficiency is calculated with the equation suggested by Gameson (1957):

$$E = \frac{c_d - c_u}{c_s - c_u} = 1 - \frac{1}{\exp\left(k \times a \times t\right)} \tag{4.1}$$

In Eq. 4.1, E denotes aeration efficiency, which has a range between 0, for no aeration, to 1, for total downstream saturation. C_u and C_d are the DO concentrations upstream and

downstream of a hydraulic structure, respectively; C_s saturation concentration of dissolved oxygen for a given ambient condition; K air-water mass transfer coefficient m/s; a, air-water contact area per unit volume (m^2 /m^3); and t bubble residence time (sec).

According to the surface renewal theory, the mass transfer coefficient is proportional to the square root of the surface-renewal frequency, which originated from energy containing large-scale eddies. At different temperatures, the physical and chemical properties of water change. This in turn will influence the air-water gas transfer rate. Self aeration efficiency is therefore converted to a standard temperature.

4.8. Maximum Dissolved Oxygen Concentration Saturation Table

The concentration of DO in water is influenced by a number of factors, including water temperature, salinity and atmospheric pressure. The relationship between water temperature and DO is inverse: Cold water is able to "hold" more DO than warm water. The following table is based on zero salinity (for lakes), and 760 mm of Hg (1 Standard Atmosphere). Actual atmospheric pressure can be compensated for when calibrating dissolved oxygen meters by entering feet above sea level, or in some meters, an internal barometer compensates for changes in pressure automatically – provided that the barometer is properly calibrated. Dissolved oxygen values shown in the table represent "saturation" for the corresponding temperature. This value is generally used during DO meter calibration, based on the assumption that saturated conditions exist in the calibration chamber, there are no air bubbles under the membrane and no water droplets are present on the actual probe. Older analogue meters require the user to manually adjust the DO value according to the temperature; newer meters perform a self-calibration at the touch of a button and this chart is used to verify the accuracy of the calibration. If a DO value is off by more than =/- 0.3 ppm, check the probe for air bubbles or water droplets, blow off droplets and/or replace the membrane, replace the calibration chamber, and wait 15-20 minutes for the air within the chamber to be saturated with water vapour, then recalibrate. Values on the chart are also used to double-check the surface DO reading. Most surface DO readings are within 0.5 ppm of saturation, except under bloom conditions, when the lake is highly coloured, or when the atmospheric pressure is changing rapidly. If surface readings DO are off by more than 1.0 ppm, recalibration is often necessary. If surface readings are off by more than 2.0 ppm, there is most likely some problem with the probe or meter.

Table 4.1 Maximum DO Concentration Saturation Table

Temp	SatDO		Temp	SatDO		Temp	SatDO
0	14.6		5	12.8		10	11.3
0.1	14.6		5.1	12.7		10.1	11.3
0.2	14.5		5.2	12.7		10.2	11.2
0.3	14.5		5.3	12.7		10.3	11.2
0.4	14.5		5.4	12.6		10.4	11.2
0.5	14.4		5.5	12.6		10.5	11.2
0.6	14.4		5.6	12.6		10.6	11.1
0.7	14.3		5.7	12.5		10.7	11.1
0.8	14.3		5.8	12.5		10.8	11.1
0.9	14.3		5.9	12.5		10.9	11.1
1	14.2		6	12.4		11	11
1.1	14.2		6.1	12.4		11.1	11
1.2	14.1		6.2	12.4		11.2	11
1.3	14.1		6.3	12.4		11.3	11
1.4	14.1		6.4	12.3		11.4	10.9
1.5	14		6.5	12.3		11.5	10.9
1.6	14		6.6	12.3		11.6	10.9
1.7	13.9		6.7	12.2		11.7	10.9
1.8	13.9		6.8	12.2		11.8	10.8
1.9	13.9		6.9	12.2		11.9	10.8
2	13.8		7	12.1		12	10.8
2.1	13.8		7.1	12.1		12.1	10.8
2.2	13.8		7.2	12.1		12.2	10.7
2.3	13.7		7.3	12.1		12.3	10.7
2.4	13.7		7.4	12		12.4	10.7
2.5	13.6		7.5	12		12.5	10.7
2.6	13.6		7.6	12		12.6	10.6
2.7	13.6		7.7	11.9		12.7	10.6
2.8	13.5		7.8	11.9		12.8	10.6
2.9	13.5		7.9	11.9		12.9	10.6
3	13.5		8	11.8		13	10.5
3.1	13.4		8.1	11.8		13.1	10.5
3.2	13.4		8.2	11.8		13.2	10.5
3.3	13.4		8.3	11.8		13.3	10.5
3.4	13.3		8.4	11.7		13.4	10.4
3.5	13.3		8.5	11.7		13.5	10.4
3.6	13.2		8.6	11.7		13.6	10.4
3.7	13.2		8.7	11.6		13.7	10.4
3.8	13.2		8.8	11.6		13.8	10.4
3.9	13.1		8.9	11.6		13.9	10.3
4	13.1		9	11.6		14	10.3
4.1	13.1		9.1	11.5		14.1	10.3
4.2	13		9.2	11.5		14.2	10.3
4.3	13		9.3	11.5		14.3	10.2
4.4	13		9.4	11.5		14.4	10.2
4.5	12.9		9.5	11.4		14.5	10.2
4.6	12.9		9.6	11.4		14.6	10.2
4.7	12.9		9.7	11.4		14.7	10.2
4.8	12.8		9.8	11.3		14.8	10.1
4.9	12.8		9.9	11.3		14.9	10.1

Temp	SatDO		Temp	SatDO		Temp	SatDO
15	10.1		20	9.1		25	8.3
15.1	10.1		20.1	9.1		25.1	8.2
15.2	10		20.2	9.1		25.2	8.2
15.3	10		20.3	9		25.3	8.2
15.4	10		20.4	9		25.4	8.2
15.5	10		20.5	9		25.5	8.2
15.6	10		20.6	9		25.6	8.2
15.7	9.9		20.7	9		25.7	8.2
15.8	9.9		20.8	9		25.8	8.1
15.9	9.9		20.9	8.9		25.9	8.1
16	9.9		21	8.9		26	8.1
16.1	9.8		21.1	8.9		26.1	8.1
16.2	9.8		21.2	8.9		26.2	8.1
16.3	9.8		21.3	8.9		26.3	8.1
16.4	9.8		21.4	8.8		26.4	8.1
16.5	9.8		21.5	8.8		26.5	8
16.6	9.7		21.6	8.8		26.6	8
16.7	9.7		21.7	8.8		26.7	8
16.8	9.7		21.8	8.8		26.8	8
16.9	9.7		21.9	8.8		26.9	8
17	9.7		22	8.7		27	8
17.1	9.6		22.1	8.7		27.1	8
17.2	9.6		22.2	8.7		27.2	7.9
17.3	9.6		22.3	8.7		27.3	7.9
17.4	9.6		22.4	8.7		27.4	7.9
17.5	9.6		22.5	8.7		27.5	7.9
17.6	9.5		22.6	8.6		27.6	7.9
17.7	9.5		22.7	8.6		27.7	7.9
17.8	9.5		22.8	8.6		27.8	7.9
17.9	9.5		22.9	8.6		27.9	7.8
18	9.5		23	8.6		28	7.8
18.1	9.4		23.1	8.6		28.1	7.8
18.2	9.4		23.2	8.5		28.2	7.8
18.3	9.4		23.3	8.5		28.3	7.8
18.4	9.4		23.4	8.5		28.4	7.8
18.5	9.4		23.5	8.5		28.5	7.8
18.6	9.4		23.6	8.5		28.6	7.7
18.7	9.3		23.7	8.5		28.7	7.7
18.8	9.3		23.8	8.5		28.8	7.7
18.9	9.3		23.9	8.4		28.9	7.7
19	9.3		24	8.4		29	7.7
19.1	9.3		24.1	8.4		29.1	7.7
19.2	9.2		24.2	8.4		29.2	7.7
19.3	9.2		24.3	8.4		29.3	7.7
19.4	9.2		24.4	8.4		29.4	7.6
19.5	9.2		24.5	8.3		29.5	7.6
19.6	9.2		24.6	8.3		29.6	7.6
19.7	9.1		24.7	8.3		29.7	7.6
19.8	9.1		24.8	8.3		29.8	7.6
19.9	9.1		24.9	8.3		29.9 & 30	7.6

CHAPTER 5

5.1. Objectives

The study reported herein is based on experiments carried out in the Fluvial Hydraulics Laboratory of the School of Water Resources Engineering at Jadavpur University using a physical hydraulic model. The study is confined to a rectangular flume. In the present study following attempts have been made-

- To observe the hydraulic jump characteristics with three different sloping beds and five different discharges.
- To observe the effect of hydraulic jump on their aeration efficiency and energy dissipation.
- To check the relationship between the hydraulic jump parameters, aeration efficiency and energy dissipation rate.

5.2. Methodology

- The flume of size 0.36(W)×0.40(H)×5(L) m^3 was chosen to perform 15 numbers of hydraulic jump experiments.
- All the experiments have been carried out on the flume bed without using any bed material.
- The angle of the flume has been changed several times such as horizontal bed, 3 degrees, 6 degrees,
- The discharge for each experiment has been changed such as 15 lps, 20 lps, 25 lps, 30 lps, and 35 lps.
- Hydraulic jump is formed by adjusting the tail gate in the flume.
- Pre-jump and post-jump depths have been taken to determine the Velocity and Froude number.
- Dissolved oxygen (DO) values have been recorded using a DO meter at different points such as before the inlet gate, throughout pre-jump and post-jump and in reservoir water.
- Pre-jump velocity and post-jump velocity have been calculated.
- The inlet gate opening has been kept fixed at 5% for all the experiments.
- Outlet gate opening is measured.
- Pre-jump and Post-jump Froude numbers have been calculated.
- Jump lengths have been calculated.
- Pre-jump energy, post-jump energy and energy losses have been calculated.
- Aeration efficiency has been calculated.

CHAPTER 6

6.1. Experimental Setup

Typical investigation of dissolved oxygen measurements has been taken several times with varying discharge and varying slope. All the experiments are conducted in the Fluvial Hydraulics laboratory of the School of Water Resources Engineering, Jadavpur University, Kolkata. The different components of the experimental set-up are illustrated and described below-

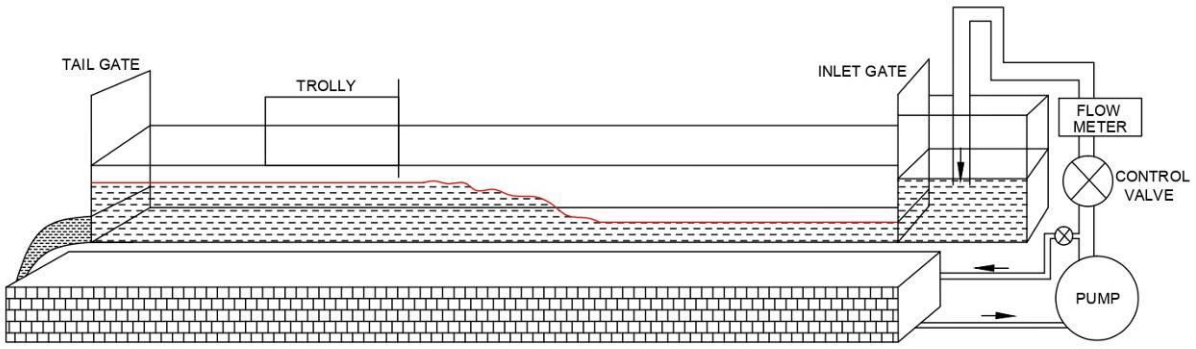

Fig. 6.1. Schematic diagram of the flume.

6.1.1. Flume

The experiments are carried out in a rectangular flume (Fig. 6.2) of 5 m long, 0.36 m wide, and 0.4(m) depth. It can tilt upto 9°.

Fig. 6.2. Tilting flume.

6.1.2. Pump

The hydraulic machines which convert the mechanical energy into hydraulic energy are called pumps. Hydraulic energy is in the form of pressure energy. The pump is made by Kirloskar Brothers Limited which is a three-phase induction motor. The rectangular flow system is served with a 15 hp, variable speed, centrifugal pump located at the upstream end of the flume. The rpm of the pump is 1850; maximum discharge is 60 lps, power 11 kW. Figure 6.2 shows the centrifugal pump.

Fig. 6.2. Centrifugal pump.

6.1.3. Reservoir

Figure 6.3. shows a reservoir with a size of 4.7(m)×0.6(m)×0.72(m) to store the water for the experiment. It was made of concrete.

Fig. 6.3. Reservoir.

6.1.4. DO Meter

We have used a DO METER of HACH company to measure the dissolved oxygen before the inlet gate, pre-jump, post jump and reservoir. DO is measured in milligrams per litre. It has a range of 0.1 to 20.0 mg/l (ppm) 1 to 200% saturation. Its accuracy ±0.1 mg/l for 0 to 8 mg/l ±0.2 mg/l for greater than 8 mg/l. The operating temperature is 0 to 50°C (32 to 122 °*F*). Its minimum sample depth is 25 mm (0.984). Figure 6.3. shows the DO meter.

Fig. 6.3. DO meter.

6.1.5. Inlet Gate

In front of the flume, there is an inlet gate to control the flow of water which has a 0.7(m)×0.36(m) dimension. Figure 6.4. shows the inlet gate.

Fig. 6.4. Inlet gate.

6.1.6. Outlet Gate

At the end of the flume, there is an outlet gate to control the outflow of water from the flume which has a 0.4(m)×0.36(m) dimension. Figure 6.5 shows the outlet gate.

Fig. 6.5. Outlet gate.

6.1.7. Point Gauge

There is a point gauge to measure the water depth at pre-jump and post-jump locations. Figure 6.6. shows the point gauge.

Fig. 6.6. Meter gauge

6.1.8. Flow meter

There is a flow meter of Endress+Hauser company, its temperature limit is -10°C to +50°C or +14°F to +122°F. Figure 6.7 shows the flow meter used in the laboratory.

Fig. 6.7. Flow meter

6.1.9. Experimental Chart

Table 6.1. Experimental chart showing the inputs and outputs

Exp-eriment No	Q (m^3/s)	Slope (θ)	Pre jump depth (m)	Post jump depth (m)	Pre jump Froude no	Post jump Froude no	U/S vel (m/s)	D/S vel (m/s)	Aeration efficiency (%)	Jump length (m)	Energy loss (m)	E1 (m)	% of initial energy lost	(Pre-Jump/ Post-jump)
1	15	0°	0.03	0.08	2.09	0.53	1.28	0.51	12.50	0.34	0.01	0.12	9.48	0.40
2	20	0°	0.03	0.12	3.05	0.40	1.77	0.46	11.76	0.62	0.05	0.19	24.65	0.26
3	25	0°	0.03	0.14	4.00	0.34	2.48	0.48	15.00	0.88	0.10	0.34	28.72	0.19
4	30	0°	0.02	0.20	6.90	0.25	3.79	0.41	15.79	1.24	0.33	0.75	44.02	0.11
5	35	0°	0.02	0.21	6.63	0.25	4.05	0.46	18.37	1.31	0.33	0.86	38.65	0.11
6	35	3°	0.02	0.27	8.41	0.22	4.05	0.36	38.09	1.73	0.67	0.86	77.91	0.09
7	30	3°	0.03	0.23	5.17	0.24	3.28	0.36	29.17	1.45	0.42	0.57	72.51	0.11
8	25	3°	0.03	0.20	5.11	0.29	2.39	0.36	40.00	1.23	0.19	0.32	57.79	0.15
9	20	3°	0.03	0.19	5.10	0.29	1.98	0.30	34.78	1.18	0.10	0.23	43.02	0.15
10	15	3°	0.05	0.16	2.50	0.46	0.81	0.26	60.00	0.74	0.04	0.08	44.21	0.32
11	15	6°	0.03	0.15	4.00	0.35	1.39	0.28	77.78	0.97	0.08	0.13	60.32	0.20
12	20	6°	0.03	0.14	3.62	0.36	1.85	0.39	72.22	0.78	0.14	0.21	66.69	0.22
13	25	6°	0.03	0.22	5.34	0.28	2.24	0.32	73.68	1.43	0.21	0.29	74.28	0.14
14	30	6°	0.03	0.15	3.72	0.36	2.62	0.55	58.36	0.83	0.30	0.38	78.60	0.21
15	35	6°	0.03	0.22	6.43	0.05	3.90	0.45	68.75	1.40	0.72	0.80	89.97	0.12

CHAPTER 7

7.1 Results and Discussion

In this study, 15 numbers of experiments have been carried out with the flume.

7.1.1 Experiment No 1

The first experiment was carried out with the flume and do meter in the horizontal bed of 15 lps discharge.

Horizontal bed
Discharge = 15 lps
Inlet gate opening = 4 cm.

Reservoir DO= 5.04 mg/l
DO before inlet = 7.20 mg/l
Outlet gate opening = 5.5 cm.

Fig 7.1. Horizontal bed 15 lps discharge

Here we have experimented in the horizontal bed in 15 lps discharge. We measured DO before the inlet gate which was 7.20 mg/l and reservoir DO before starting the experiment which was 5.04 mg/l. **Figure 7.1.** shows the hydraulic jump formed during the experiment.

7.1.2. Experiment No 2

Horizontal bed
Discharge = 20 lps.
Inlet gate Opening = 4 cm

Reservoir DO = 5.2 mg/l
DO before inlet gate = 7.09 mg/l
Outlet gate Opening = 5 cm.

Fig. 7.2. Horizontal bed 20 lps discharge

Here we have done the experiment in the horizontal bed in 20 lps discharge. We measured DO before the inlet gate which was 7.09 mg/l and reservoir DO before starting the experiment which was 5.20 mg/l. **Figure 7.2.** shows the hydraulic jump formed during the experiment.

7.1.3 Experiment No 3

Horizontal bed — Reservoir DO = 5.6 mg/l
Discharge = 25 lps. — DO before inlet gate = 7.18 mg/l
Inlet gate Opening= 4 cm. — Out let gate Opening = 5.5 cm

Fig. 7.3. Horizontal bed 25 lps discharge

Here we have experimented in the horizontal bed in 25 lps discharge. We measured DO before the inlet gate which was 7.18 mg/l and reservoir DO before starting the experiment which was 5.6 mg/l. **Figure 7.3.** shows the hydraulic jump formed during the experiment.

7.1.4. Experiment No 4

Horizontal bed — Reservoir DO = 5.26 mg/l
Discharge = 30 lps — DO before inlet gate opening = 7.35 mg/l
Inlet Gate Opening = 4 cm. — Outlet Gate Opening =7.3 cm.

Fig. 7.4. Horizontal bed 30 lps discharge

Here we have done the experiment in the horizontal bed in 30 lps discharge. We measured dissolved oxygen (DO) before the inlet gate which was 7.35 mg/l and reservoir DO before

starting the experiment which was 5.26 mg/l. **Figure 7.4.** shows the hydraulic jump formed during the experiment.

7.1.5. Experiment No 5

Horizontal bed
Discharge = 35 lps.
Inlet Gate Opening = 4 cm.

Reservoir DO = 7.5mg/L
DO before inlet gate = 7.03 mg/L
Outlet Gate Opening = 8 cm.

Fig. 7.5. Horizontal bed 35 lps discharge

Here we have done the experiment in the horizontal bed in 35 lps discharge. We measured DO before the inlet gate which was 7.03 mg/l and reservoir DO before starting the experiment which was 7.5 mg/l. **Figure 7.5.** shows the hydraulic jump formed during the experiment.

7.1.6. Experiment No 6

3° slope bed
Discharge= 35 lps .
Inlet Gate Opening= 4 cm.

Reservoir DO = 5.50 mg/L
DO before inlet gate opening = 7.10 mg/L
Outlet Gate Opening = 5.6 cm.

Fig. 7.6. 3° slope bed 35 lps discharge

Here we have done the experiment on the a 3° bed slope in 35 lps discharge. We measured the DO before the inlet gate which was 7.10 mg/l and reservoir DO before starting the experiment which was 5.50 mg/l. **Figure 7.6.** shows the hydraulic jump formed during the experiment.

7.1.7. Experiment No 7

3° slope bed
Discharge = 30 lps.
Inlet Gate Opening = 4 cm.
Reservoir DO = 4.52 mg/l
DO before inlet gate opening = 7.34 mg/l
Outlet Gate Opening = 5.5 cm.

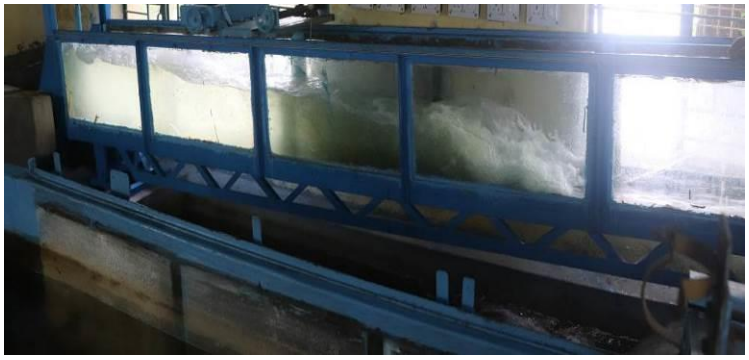

Fig. 7.7. 3° slope bed 30 lps discharge

Here we have done the experiment on a 3° bed slope in 30 lps discharge. We measured the DO before the inlet gate which was 7.34 mg/l and reservoir DO before starting the experiment which was 4.52 mg/l. **Figure7.7.** shows the hydraulic jump formed during the experiment.

7.1.8. Experiment No 8

3° slope bed
Discharge = 25 lps.
Inlet Gate Opening = 4 cm.
Reservoir DO = 5.52 mg/l
DO before inlet gate opening = 7.30 mg/l
Outlet Gate Opening = 4.2 cm

Fig. 7.8. 3° slope bed 25 lps discharge

Here we have done the experiment on a 3° bed slope in 25 lps discharge. We measured the DO before the inlet gate which was 7.30 mg/l and reservoir DO before starting the experiment which was 5.52 mg/l. **Figure 7.8** shows the hydraulic jump formed during the experiment.

7.1.9. Experiment No 9

3° slope bed
Discharge = 20 lps.
Inlet Gate Opening = 4 cm.
Reservoir DO = 5.21 mg/l
DO before inlet gate opening = 7.50 mg/l
Outlet Gate Opening = 3.5 cm.

Fig. 7.9. 3° slope bed 20 lps discharge

Here we have done the experiment on a 3° bed slope in 20 lps discharge. We measured the DO before the inlet gate which was 7.50 mg/l and reservoir DO before starting the experiment which was 5.21 mg/l. **Figure 7.9** shows the hydraulic jump formed during the experiment.

7.1.10. Experiment No 10

3° slope bed
Discharge = 15 lps.
Inlet Gate Opening = 4 cm.
Reservoir DO = 5.21 mg/l
DO before inlet gate opening = 7.32 mg/l
Outlet Gate = 3 cm.

Fig. 7.10. 3° slope bed 15 lps discharge

Here we have done the experiment on a 3° bed slope in 15 lps discharge. We measured the DO before the inlet gate which was 7.32 mg/l and reservoir DO before starting the

experiment which was 5.21 mg/l. **Figure 7.10** shows the hydraulic jump formed during the experiment.

7.1.11. Experiment No 11

6° slope bed
Discharge = 35 lps.
Inlet Gate Opening = 4 cm.
Reservoir DO = 4.7 mg/l
DO before inlet gate opening = 7.46 mg/l
Outlet Gate Opening = 2.5 cm

Fig. 7.11. 6° slope bed 15 lps discharge

Here we have done the experiment on a 6° bed slope in 15 lps discharge. We measured the DO before inlet gate which was 7.46 mg/l and reservoir DO before starting the experiment which was 4.7 mg/l. **Figure 7.11** shows the hydraulic jump formed during the experiment.

7.1.12. Experiment No 12

6° slope bed
Discharge = 20 lps.
Inlet gate Opening = 4 cm.
Reservoir DO = 4.70 mg /L
DO before inlet gate opening = 7.29 mg/L
Outlet gate Opening = 3 cm.

Fig.7.12. 6° slope bed 20 lps discharge

Here we have experimented on a 6° bed slope in 20 lps discharge. We measured the DO before the inlet gate which was 7.29 mg/l and reservoir DO before starting the experiment which was 4.7 mg/l. **Figure 7.12** shows the hydraulic jump formed during the experiment.

7.1.13. Experiment No 13

6° slope bed
Reservoir DO = 4.93 mg/l

Discharge = 25 lps. DO before inlet gate opening = 7.42 mg/l
Inlet Gate Opening = 4 cm Outlet Gate Opening = 3.8 cm.

Fig. 7.13. 6° slope bed 25 lps discharge

Here we have done the experiment on a 6° bed slope in 25 lps discharge. We measured the DO before the inlet gate which was 7.42 mg/l and reservoir DO before starting the experiment which was 4.93 mg/l. **Fig.7.13.** shows the experiment.

7.1.14. Experiment No 14

6° slope bed Reservoir DO = 5.00 mg/l
Discharge = 30 lps. DO before inlet gate opening = 7.30 mg/l
Inlet Gate Opening = 4 cm. Outlet Gate Opening = 5.8 cm.

Fig. 7.14. 6° slope bed 30 lps discharge.

Here we have done the experiment on a 6° bed slope in 30 lps discharge. We measured the DO before the inlet gate which was 7.30 mg/l and reservoir DO before starting the experiment which was 5.00 mg/l. **Figure 7.14** shows the hydraulic jump formed during the experiment.

7.1.15. Experiment No 15

6° slope bed Reservoir DO = 5.00 mg/l
Discharge = 35 lps. DO before inlet gate opening = 7.30 mg/l
Inlet Gate Opening = 4 cm.
Outlet Gate Opening = 6 cm

Fig. 7.15. 6° slope bed 35 lps discharge

Here we have done the experiment on a 6° bed slope in 35 lps discharge. We measured dissolved oxygen (DO) before the inlet gate which was 7.30 mg/l and reservoir DO before starting the experiment which was 5.00 mg/l. **Fig. 7.15.** shows the hydraulic jump formed during the experiment.

7.2. Experimental Outcomes

The flume was chosen to perform 15 numbers of hydraulic jump experiments to measure dissolved oxygen changes using a DO meter. All these experiments were conducted at different discharges and different angle of slopes. Different values of pre-jump and post-jump Froude numbers were calculated. First, five numbers of experiments were conducted on the horizontal flume bed. It was found that the obtained results are convenient with Gameson's equation (4.1). Experimental runs were carried out to study the different characteristics of the hydraulic jump such as sequent depth ratio, jump height, relative length of the jump, and relative energy loss, at different Froude numbers for different bed slopes. Also, other experimental runs were conducted with different slopes and discharges. According to the recorded readings, we have plotted many graphs as shown in **Figs. 7.16-7.21**.

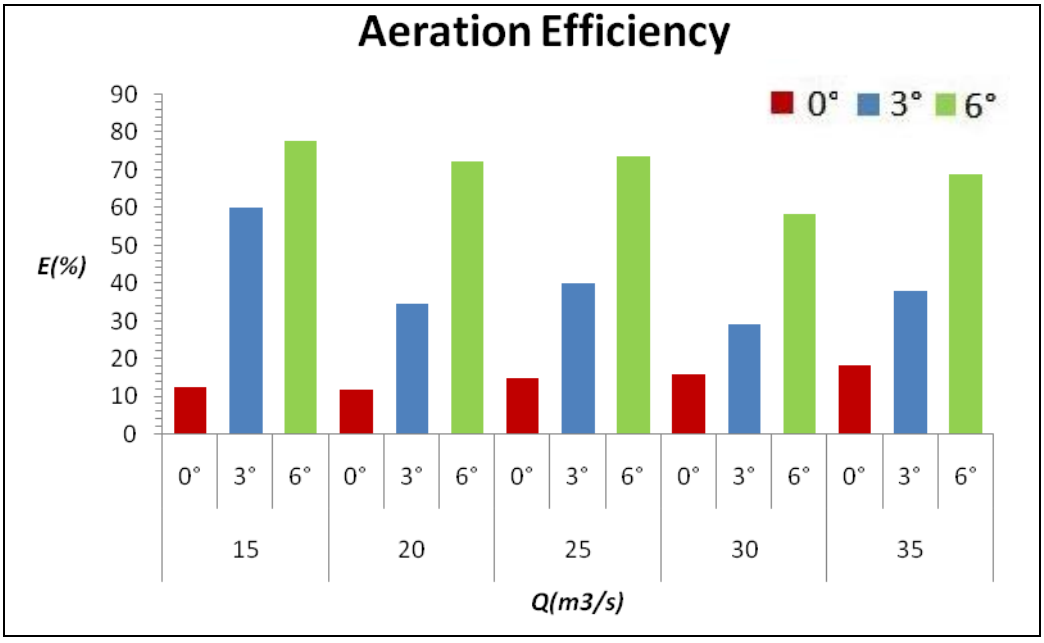

Fig. 7.16. Aeration efficiency varying with discharge and slope.

In **Fig. 7.16** a graph of aeration efficiency vs discharge at different bed slopes has been plotted. We can see that for a given discharge, aeration efficiency increases with increasing slope. In **Fig. 7.16**, the bars, plotted in red colour, represent 0° slope; blue colour bars represent 3° slope and green colour bars represent 6° slope.

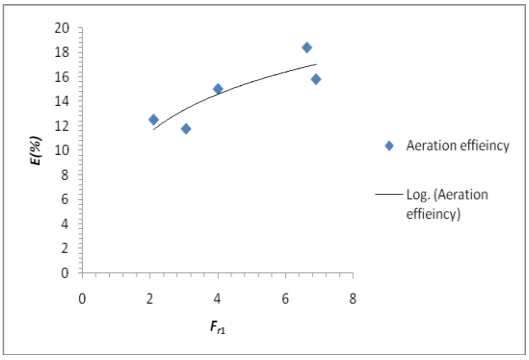

Fig.7.17(a)

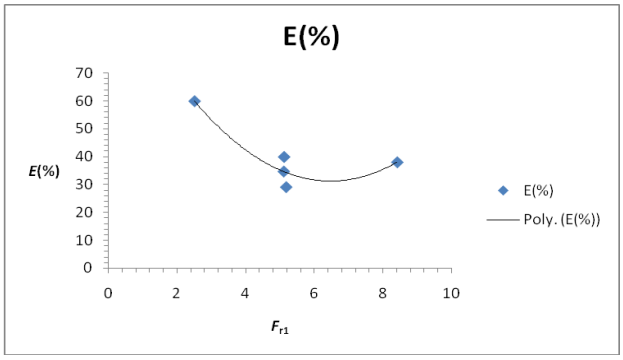

Fig. 7.17.(b)

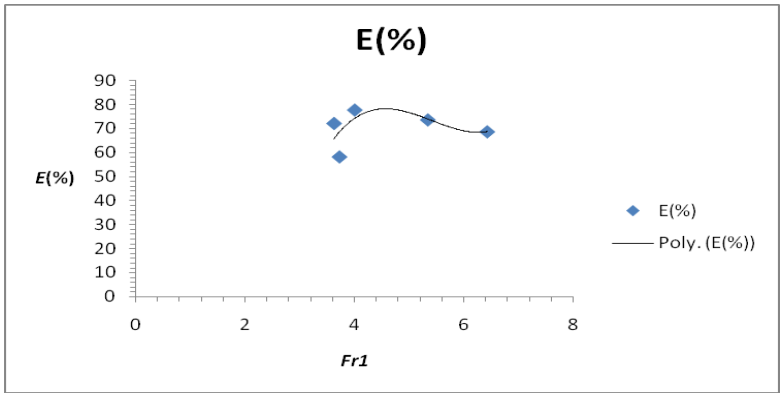

Fig. 7.17.(c). Variation of aeration efficiency with the pre-jump Froude number.

In **Fig. 7.17(a,b,c),** we have shown the variation in aeration efficiency with changes in the pre-jump Froude number. **Fig. 7.17(a,b,c)** represents the graph for bed slope 0^0, 3^0 and 6^0 respectively. In the graph, Y-axis shows the aeration efficiency in percentage and the X-axis shows the pre-jump Froude number.

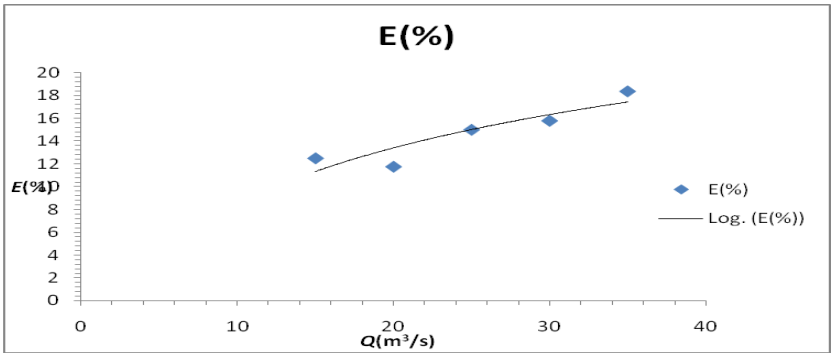

Fig.7.18.(a) Discharge versus aeration efficiency.

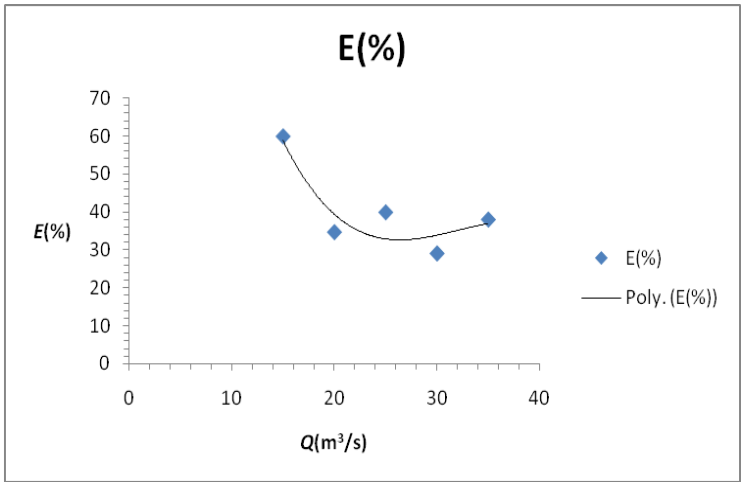

Fig.7.18.(b) Discharge versus aeration efficiency.

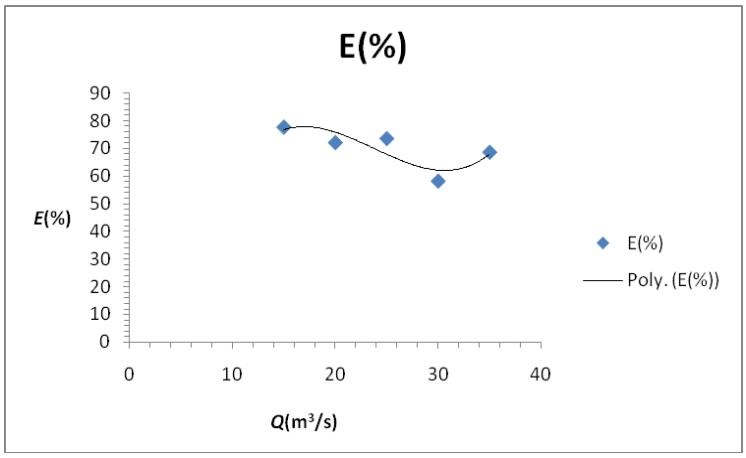

Fig.7.18.(c) Discharge versus aeration efficiency.

The variation of aeration efficiency with discharge is shown in **Fig. 7.18.**(a),(b),(c), where, the graphs have been plotted with aeration efficiency vs discharge. **Fig. 7.18(a,b,c)** represents the graph for bed slope 0^0, 3^0 and 6^0 respectively. The variation of aeration efficiency with discharge is not clear from **Fig. 7.18 (a, b, c)**, as the three graph shows different trends.

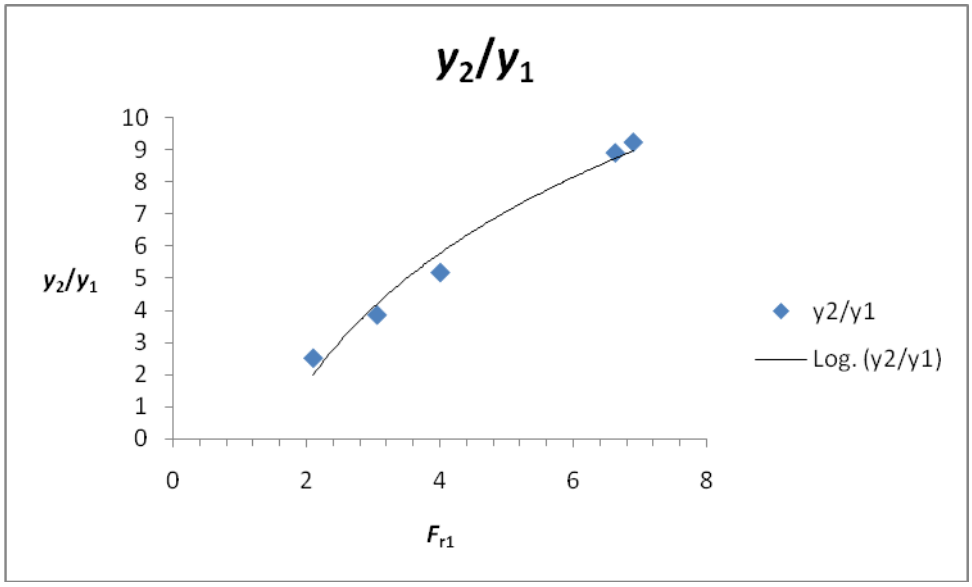

Fig.7.19.(a) 0° slope pre-jump Froude number versus sequent depth.

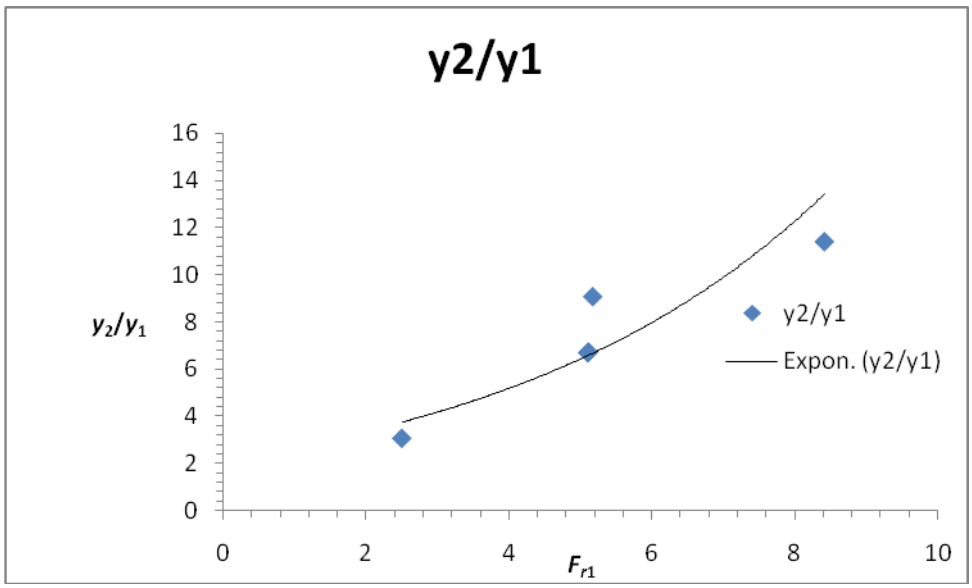

Fig.7.19.(b) 3° Slope pre-jump Froude number versus sequent depth.

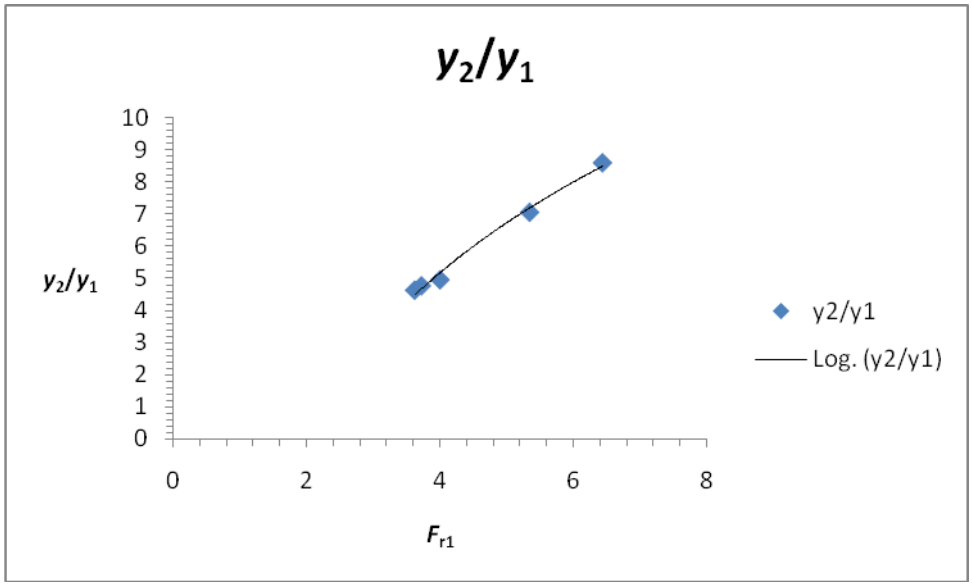

Fig.7.19.(c).6° Pre-jump Froude number versus sequent depth.

Graphs are plotted to study the relationship between the hydraulic jump sequent depth ratio, y_2/ y_1 and Froude's number, F_1 as can be seen in **Fig. 7.19.(a, b, c).** These figures show that the sequent depth ratio, $\boldsymbol{y}_2 / \boldsymbol{y}_1$ increases as the Froude number (F_1) increases.

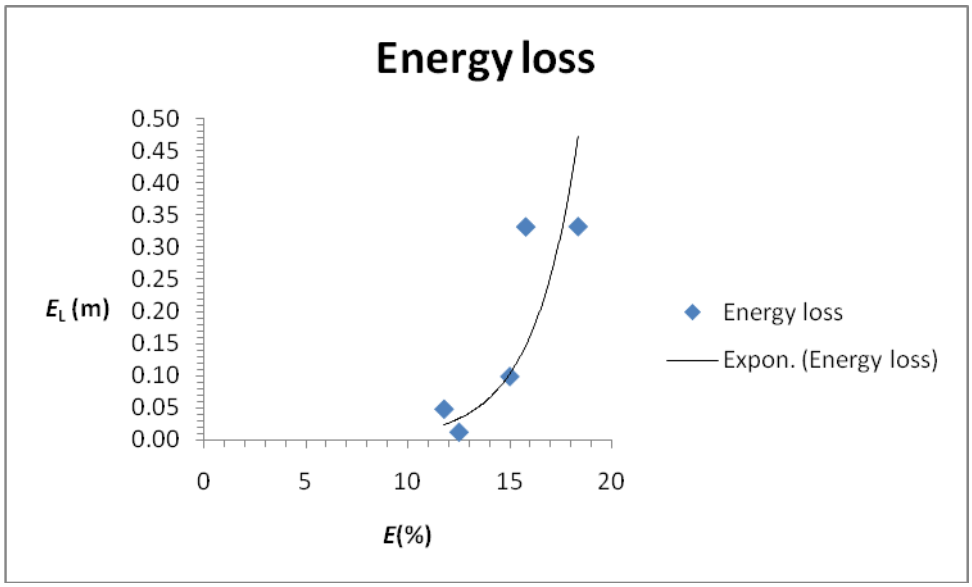

Fig.7.20.(a) 0° slope aeration efficiency versus energy loss.

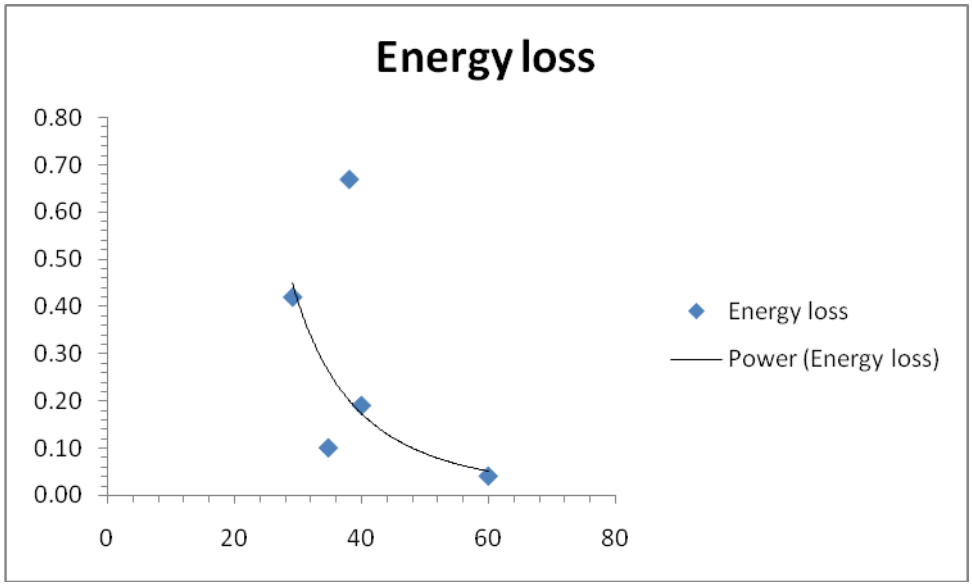

Fig.7.20.(b) 3° slope aeration efficiency versus energy loss.

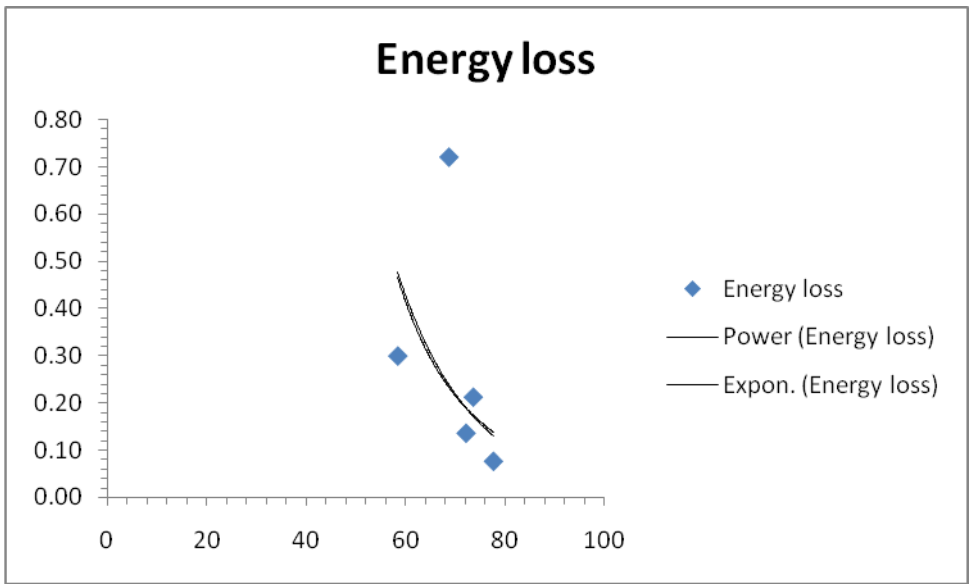

Fig.7.20(c) 6° slope aeration efficiency versus energy loss.

In **Fig.7.20.(a),(b),(c)** aeration efficiency versus energy losses graphs have been plotted.

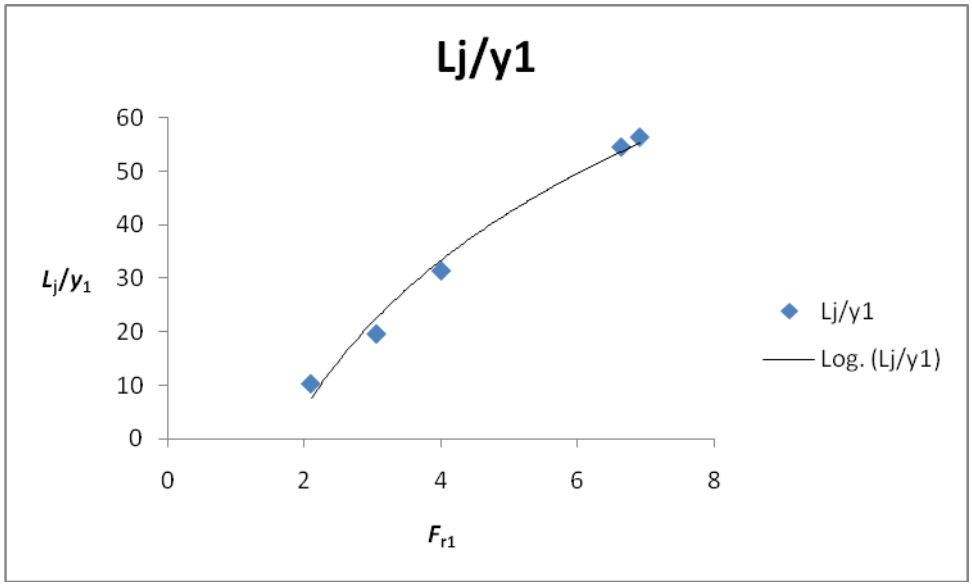

Fig.7.21.(a) 0° slope pre-jump Froude number versus hydraulic jump length ratio.

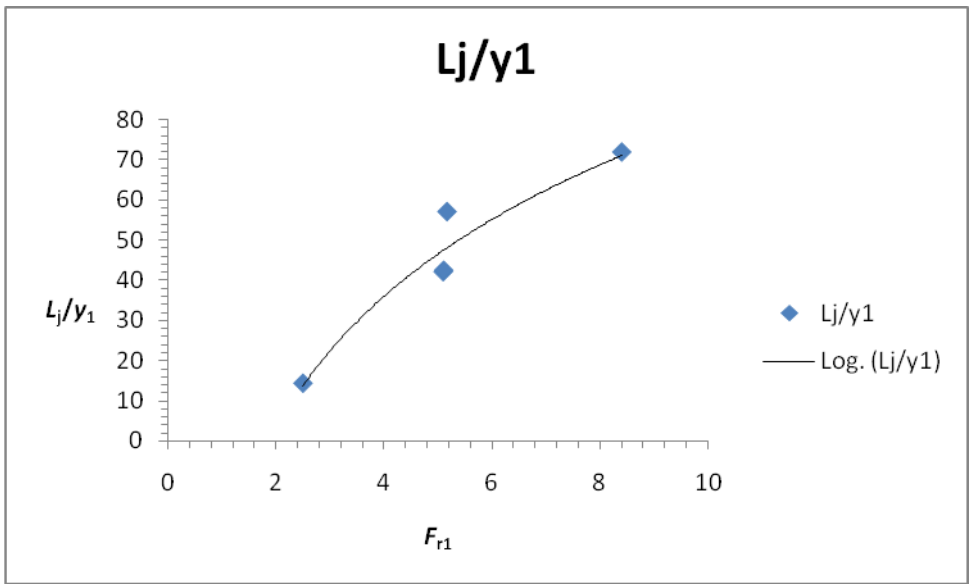

Fig.7.21.(b) 3° slope pre-jump Froude number versus hydraulic jump length ratio.

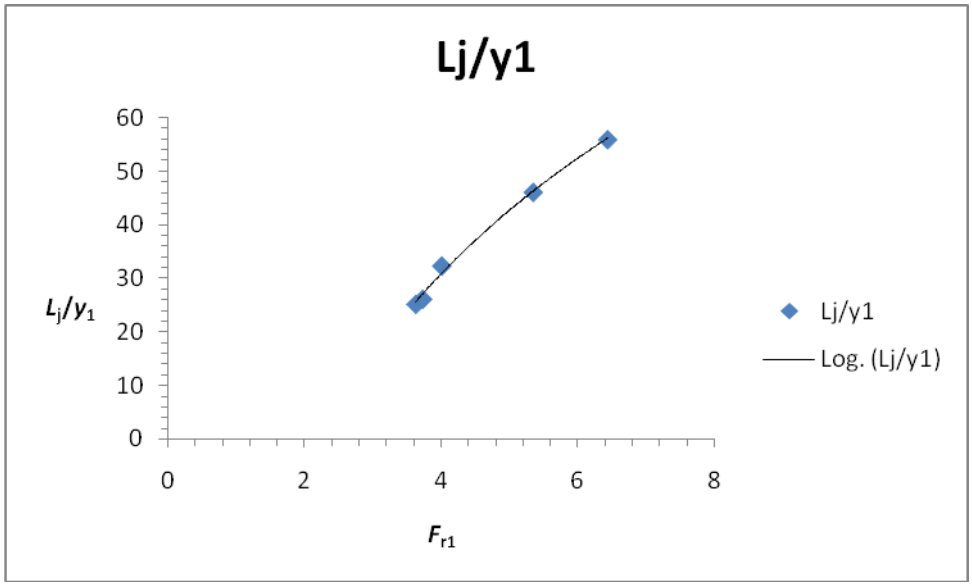

Fig.7.21(c) 6° slope pre-jump Froude number versus hydraulic jump length ratio.

In **Fig. 7.21.(a),(b),(c)** pre-jump Froude numbers versus non-dimensional hydraulic jump length have been plotted for different slopes. It can be seen that jump length increases with increasing prejump Froude number.

The main aim of this work was to investigate aeration efficiency, and from all the experiments it can be seen that aeration takes place in the hydraulic jump and it can be termed as significant. Most importantly we can say that significant aeration takes place in hydraulic jump and it can be increased by increasing the bed slope. From **Fig. 7.16**, it can be seen that for the same discharge the aeration efficiency is more for the higher bed slope. However, no specific trend of aeration efficiency with prejump Froude number is found.

CHAPTER 8

8.1. Conclusion

The results show that hydraulic jump length in terms of pre-jump Froude number, F_1, provides information to estimate hydraulic jump lengths at different channel bed slopes. Experimental results of this work conclude that the sequent depth for the hydraulic jump estimation has to take the channel bed slope into account. The sequent depth ratio, y_2/y_1 increases as the initial Froude number and channel bed slope increase.
The scope of the study was also to analyse the different similarities of air entrainment in hydraulic jumps and to discuss current practices. The measured DO data are re-examined and scrutinised to investigate the DO exchange phenomena through an air-water interface. In particular, oxygen transfer efficiency, hydraulic jump, pre-jump Froude number, post-jump Froude number, and jump length are discussed. In this experimental study, the aeration performance of a hydraulic jump has been investigated by means of energy losses.

8.2. Notation

A = Area of the rectangular flume [L^2]

C_u = Upstream dissolved oxygen concentration [ML^{-3}]

C_d = Down-stream dissolved oxygen concentration [ML^{-3}]

C_s = Saturation Dissolved oxygen concentration [ML^{-3}]

E_1 = Upstream energy [L]

E_2 =Down-stream energy [L]

Fr_1 =Up-stream Froude number

Fr_2 = Down-stream Froude number

Fs= Shear force on the control surface adjacent to the channel boundary [MLT^{-2}]

H_1 = Total energy at section 1[M]

H_2 =Total energy at section 2[M]

Lj = Jump length[M]

M_1 = Momentum flux in the longitudinal direction going in through the control surface [MLT^1]

M_2 = Momentum flux in the longitudinal direction going out through the control surface [MLT^{-1}]

P_1 = Pressure force at the control surface at Section 1= $\gamma A_1 \bar{y}_1 \cos\theta$ by assuming hydrostatic pressure distribution, where y_1 = depth of the centroid of the area below the water surface. [$ML^{-1}T^{-2}$]

P_2 = Pressure force at the control surface at Section 1= $\gamma A_2 \bar{y}_2 \cos\theta$ by assuming hydrostatic pressure distribution, where y_2 = depth of the centroid of the area below the water surface. . [$ML^{-1}T^{-2}$]

Q = Discharge [L^3T^{-1}]

q = Discharge per width [L^2T^{-1}]

T = Top width of flume [L]

V_1 = Upstream velocity [LT^{-1}]

V_2 = Downstream velocity [LT^{-1}]

$W \sin \theta$ = longitudinal component of the weight of water contained in the control volume [MLT^{-2}]

x = Horizontal distance [L]

y_1 =Up stream depth [L]

y_2 = Downstream depth [L]

8.3. Reference

Bostan, T., Coşar, A., Yetilmezsoy, K., Topçu, S., & Ağaççıoğlu, H. (2013). The effect of hydraulic jump on the aeration efficiency. *2nd International Balkans Conference on Challenges of Civil Engineering, BCCCE,* Epoka University, Tirana, Albania.

Bai, R., Ning, R., Liu, S., & Wang, H. (2022). Hydraulic jump on a partially vegetated bed. *Water Resources Research*, 58(7), e2022WR032013.

Bidone, P. G. (1820). Experiences Sur Le Remou Et Sur La Propagation Des Ondes. (in French). Turin. de l'Imprimerie Royale. https://gutenberg.beic.it/webclient/DeliveryManager?pid=750810&custom_att_2=simple_viewer&search_terms=DTL3&pds_handle=

Bradley, J N and Peterka, A J(1957) 'The Hydraulic Design of Stilling Basins, Hydraulic Jumps on a Horizontal Apion', *Journal of Hydraulic Divisions*, Proc. ASCE, Paper No. 1401, pp 1401–l–25.

Chanson, H., & Toombes, L. (2002). Air–water flows down stepped chutes: turbulence and flow structure observations. *International Journal of Multiphase Flow*, *28*(11), 1737-1761.

Eltoukhy, M. A. R. (2016). Hydraulic jump characteristics for different open channel and stilling basin layouts. *International Journal of Civil Engineering and Technology*, *7*(2), 290-301.

Elevatorski, E A,(1959) Hydraulic Energy Dissipators, McGraw-Hill, New York.

Hoque, A., & Paul, A. K. (2022). Experimental investigation of oxygen transfer efficiency in hydraulic jumps, plunging jets, and plunging breaking waves. *Water Supply*, *22*(4), 4320-4333.

Jaiswal, A., & Goel, A. (2019). Aeration through weirs— a critical review. *Sustainable Engineering*, 187-200.

Kim, J., Kim, S., & Li, M. J. (2016, January). Oxygen Transfer and Energy Dissipation by Nappe and Skimming Flow over Stepped Weir Structure. In *International Conference on Education, Management, Computer and Society* (pp. 1691-1695). Atlantis Press.

Kucukali, S. E. R. H. A. T., & Cokgor, S. (2009). Energy concept for predicting hydraulic jump aeration efficiency. *Journal of Environmental Engineering*, *135*(2), 105-107.

Marusic, I., & Broomhall, S. (2021). Leonardo da Vinci and fluid mechanics. *Annual Review of Fluid Mechanics*, *53*, 1-25.

Pagliara, S., Carnacina, I., & Roshni, T. (2010). Self-aeration and friction over rock chutes in uniform flow conditions. *Journal of Hydraulic Engineering*, *136*(11), 959-964.

Raikar, R. V., & Kamatagi, P. B. (2015). Use of hydraulic phenomena in enhancement of dissolved oxygen concentration. *Int J Res Eng Technol*, *4*(2).

Rajaratnam, N,(1967) 'Hydraulic Jumps', Chapter in Advances in Hydroscience, ed. Chow, V T Vol. 4, Academic Press, New York, pp 198–280.

Rajaratnam, N and Subramanya, K,(1968) 'Profi le of the Hydraulic Jump', J. of Hyd. Div., Proc. ASCE, Paper No. 5931, pp 663–673.

Standard Method for the Examination of Water and Wastewater, Marine Volunteer Lake Monitoring Program, 24 Maple Hill Road, Auburn city of Alabama, ME 04210.

Subramanya, K,(1967) 'Some Studies on Turbulent Wall Jets in Hydraulic Engineering', Ph. D. thesis, Univ. of Alberta, Edmonton, Canada, Oct.

Toombes, L., & Chanson, H. (2005). Air–water mass transfer on a stepped waterway. *Journal of Environmental Engineering*, *131*(10), 1377-1386.

Wilhelms, S. C., & Smith, D. R. (1981). Reaeration through gated-conduit outlet works.

Wilhelms, S. C., Gulliver, J. S., & Parkhill, K. (1993). Reaeration at low-head hydraulic structures. Army engineer waterways experiment station vicksburg ms hydraulics lab.